$\bar{B}_c \to \eta_c$, $\bar{B}_c \to J/\psi$ and $\bar{B} \to D^{(*)}$ semileptonic decays including new physics

Neus Penalva,[1,2] Eliecer Hernández,[3] and Juan Nieves[2]

[1]*Departamento de Física Fundamental, Universidad de Salamanca, E-37008 Salamanca, Spain*
[2]*Instituto de Física Corpuscular (centro mixto CSIC-UV), Institutos de Investigación de Paterna, Apartado 22085, 46071, València, Spain*
[3]*Departamento de Física Fundamental e IUFFyM, Universidad de Salamanca, E-37008 Salamanca, Spain*

(Received 24 July 2020; accepted 4 October 2020; published 12 November 2020)

We apply the general formalism derived by Penalva *et al.* [Phys. Rev. D **101**, 113004 (2020)] to the semileptonic decay of pseudoscalar mesons containing a b quark. While present $\bar{B} \to D^{(*)}$ data give the strongest evidence in favor of lepton flavor universality violation, the observables that are normally considered are not able to distinguish between different new physics (NP) scenarios. In the above reference we discussed the relevant role that the various contributions to the double differential decay widths $d^2\Gamma/(d\omega d\cos\theta_\ell)$ and $d^2\Gamma/(d\omega dE_\ell)$ could play to this end. Here ω is the product of the two hadron four-velocities, θ_ℓ is the angle made by the final lepton and final hadron three-momenta in the center of mass of the final two-lepton system, and E_ℓ is the final charged lepton energy in the laboratory system. The formalism was applied by Penalva *et al.* to the analysis of the $\Lambda_b \to \Lambda_c$ semileptonic decay, showing the new observables were able to tell apart different NP scenarios. Here we analyze the $\bar{B}_c \to \eta_c \tau \bar{\nu}_\tau$, $\bar{B}_c \to J/\psi \tau \bar{\nu}_\tau$, $\bar{B} \to D \tau \bar{\nu}_\tau$ and $\bar{B} \to D^* \tau \bar{\nu}_\tau$ semileptonic decays. We find that, as a general rule, the $\bar{B}_c \to J/\psi$ observables, even including τ polarization, are less optimal for distinguishing between NP scenarios than those obtained from $\bar{B}_c \to \eta_c$ decays, or those presented by Penalva *et al.* for the related $\Lambda_b \to \Lambda_c$ semileptonic decay. Finally, we show that $\bar{B} \to D$ and $\bar{B}_c \to \eta_c$, and $\bar{B} \to D^*$ and $\bar{B}_c \to J/\psi$ decay observables exhibit similar behaviors.

DOI: 10.1103/PhysRevD.102.096016

I. INTRODUCTION

The present values of the $\mathcal{R}_{D^{(*)}}$ ratios ($\ell = e, \mu$),

$$\mathcal{R}_D = \frac{\Gamma(\bar{B} \to D\tau\bar{\nu}_\tau)}{\Gamma(\bar{B} \to D\ell\bar{\nu}_\ell)} = 0.340 \pm 0.027 \pm 0.013,$$
$$\mathcal{R}_{D^*} = \frac{\Gamma(\bar{B} \to D^*\tau\bar{\nu}_\tau)}{\Gamma(\bar{B} \to D^*\ell\bar{\nu}_\ell)} = 0.295 \pm 0.011 \pm 0.008, \quad (1)$$

are the strongest experimental evidence for the possibility of lepton flavor universality violation (LFUV). These values have been obtained by the Heavy Flavour Averaging Group (HFLAV) [1] (see also Ref. [2] for earlier results), from a combined analysis of different experimental data by the *BABAR* [3,4], Belle [5–8] and LHCb [9,10] collaborations together with standard model (SM) predictions [11–15], and they show a tension with the SM at the level of 3.1σ. However, taking only the latest Belle experiment from Ref. [8] the tension with SM predictions reduces to 0.8σ so that new experimental analyses seem to be necessary to confirm or rule out LFUV in $\bar{B}$ meson decays. Another source of tension with the SM predictions is in the ratio

$$\mathcal{R}_{J/\psi} = \frac{\Gamma(\bar{B}_c \to J/\psi\tau\bar{\nu}_\tau)}{\Gamma(\bar{B}_c \to J/\psi\mu\bar{\nu}_\mu)} = 0.71 \pm 0.17 \pm 0.18 \quad (2)$$

recently measured by the LHCb collaboration [16]. This shows a 1.8σ disagreement with SM results that are in the range $R^{\rm SM}_{J/\psi} \sim 0.25$–$0.28$ [17–29].

If the anomalies seen in the data persist, they will be a clear indication of LFUV and new physics (NP) beyond the SM will be necessary to explain it. Since the data for the two first generations of quarks and leptons is in agreement with SM expectations, NP is assumed to affect just the last quark and lepton generation. Its effects can be studied in a phenomenological way by following an effective field theory model-independent analysis that includes different $b \to c\tau\bar{\nu}_\tau$ effective operators: scalar, pseudoscalar and tensor NP terms, as well as corrections to the SM vector

and axial contributions [30]. Considering only left-handed neutrinos, in the notation of Ref. [31] one writes

$$H_{\rm eff} = \frac{4G_F|V_{cb}|^2}{\sqrt{2}}[(1+C_{V_L})\mathcal{O}_{V_L} + C_{V_R}\mathcal{O}_{V_R} + C_{S_L}\mathcal{O}_{S_L} + C_{S_R}\mathcal{O}_{S_R} + C_T\mathcal{O}_T] + \text{H.c.}, \quad (3)$$

with fermionic operators given by ($\psi_{L,R} = \frac{1\mp\gamma_5}{2}\psi$)

$$\mathcal{O}_{V_{L,R}} = (\bar{c}\gamma^\mu b_{L,R})(\bar{\ell}_L\gamma_\mu\nu_{\ell L}), \quad \mathcal{O}_{S_{L,R}} = (\bar{c}b_{L,R})(\bar{\ell}_R\nu_{\ell L}), \quad \mathcal{O}_T = (\bar{c}\sigma^{\mu\nu}b_L)(\bar{\ell}_R\sigma_{\mu\nu}\nu_{\ell L}). \quad (4)$$

The corrections to the SM are assumed to be generated by NP that enter at a much higher energy scale, and which strengths at the SM scale are governed by unknown, complex in general, Wilson coefficients [C_{V_L}, C_{V_R}, C_{S_L}, C_{S_R} and C_T in Eq. (3)] that should be fitted to data. For the numerical part of the present work, we take the values for the Wilson coefficients from the analysis carried out in Ref. [31].

The findings of these phenomenological studies show that in fact NP can solve some of the present discrepancies. However, it is also found that different combinations of NP terms could give very similar results for the $\mathcal{R}_{D^{(*)}}, \mathcal{R}_{J/\psi}$ ratios. Thus, even though those ratios are our present best experimental evidence for the possible existence of NP beyond the SM, they are not good observables for distinguishing between different NP scenarios.

The relevant role that the various contributions to the two differential decay widths $d^2\Gamma/(d\omega d\cos\theta_\ell)$ and $d^2\Gamma/(d\omega dE_\ell)$ could play to this end was analyzed in detail in Refs. [32,33]. Here, ω is the product of the two hadron four-velocities, θ_ℓ is the angle made by the final lepton and final hadron three-momenta in the center of mass of the final two-lepton pair (c.m.), and E_ℓ is the final charged lepton energy in the laboratory frame (LAB).

Even in the presence of NP, it is shown that for any charged current semileptonic decay with an unpolarized final charged lepton one can write [33]

$$\frac{d^2\Gamma}{d\omega d\cos\theta_\ell} = \frac{G_F^2|V_{cb}|^2M'^3M^2}{16\pi^3}\sqrt{\omega^2-1}\left(1-\frac{m_\ell^2}{q^2}\right)^2 A(\omega,\theta_\ell),$$

$$A(\omega,\theta_\ell) = \frac{2\bar{\sum}|\mathcal{M}|^2}{M^2(1-\frac{m_\ell^2}{q^2})}\bigg|_{\rm unpolarized} = a_0(\omega) + a_1(\omega)\cos\theta_\ell + a_2(\omega)(\cos\theta_\ell)^2, \quad (5)$$

$$\frac{d^2\Gamma}{d\omega dE_\ell} = \frac{G_F^2|V_{cb}|^2M'^2M^2}{8\pi^3}C(\omega,E_\ell),$$

$$C(\omega,E_\ell) = \frac{2\bar{\sum}|\mathcal{M}|^2}{M^2}\bigg|_{\rm unpolarized} = c_0(\omega) + c_1(\omega)\frac{E_\ell}{M} + c_2(\omega)\frac{E_\ell^2}{M^2}, \quad (6)$$

where M, M' and m_ℓ are the masses of the initial and final hadrons and the final charged lepton respectively, q^2 is the four-momentum transferred squared (related to ω via $q^2 = M^2 + M'^2 - 2MM'\omega$) and $\mathcal{M}$ is the invariant amplitude for the decay. Note that at zero recoil θ_ℓ is no longer defined and thus $a_1(\omega=1)$ and $a_2(\omega=1)$ vanish accordingly. The $a_{0,1,2}$ c.m. and $c_{0,1,2}$ LAB expansion coefficients are scalar functions that depend on ω and the masses of the particles involved in the decay. In the general tensor formalism developed in Refs. [32,33], it is shown how they are determined in terms of the 16 Lorentz scalar $\tilde{W}'s$ structure functions (SFs) that parametrize all the hadronic input. These $\tilde{W}'s$ SFs depend on the Wilson coefficients ($C's$) and the genuine hadronic responses ($W's$), the latter being scalar functions of the actual form factors that parametrize the hadronic transition matrix elements for a given decay. The general expressions for the $a_{0,1,2}$ c.m. and $c_{0,1,2}$ LAB expansion coefficients in terms of the $\tilde{W}'s$ SFs can be found in Ref. [33], where the hadron tensors associated with the different SM and NP contributions (including all possible interferences) are also explicitly given.[1]

The fully developed formalism was applied in Ref. [33] to the analysis of the $\Lambda_b \to \Lambda_c\tau\bar{\nu}_\tau$ decay. The shape of the $d\Gamma(\Lambda_b \to \Lambda_c\mu\bar{\nu}_\mu)/d\omega$ differential decay width has already been measured by the LHCb collaboration [34] and there are expectations that the $\mathcal{R}_{\Lambda_c} = \frac{\Gamma(\Lambda_b\to\Lambda_c\tau\bar{\nu}_\tau)}{\Gamma(\Lambda_b\to\Lambda_c\mu\bar{\nu}_\mu)}$ ratio may reach the precision obtained for $\mathcal{R}_D$ and $\mathcal{R}_{D^*}$ [35]. With the use of Wilson coefficients from Ref. [31], fitted to experimental data in the $\bar{B}$-meson sector, it is shown in Ref. [33] that, with the exception of a_0, all the other $a_{1,2}$ c.m. and $c_{0,1,2}$ LAB expansion coefficients are able to disentangle between different NP scenarios, i.e., different fits to the available data that otherwise give very similar values for the $\mathcal{R}_{\Lambda_c}$, and $\mathcal{R}_{D^{(*)}}$, $\mathcal{R}_{J/\psi}$ ratios, or the corresponding $d\Gamma/d\omega$ distributions.

In this work we apply the general formalism of Ref. [33] to the study of the semileptonic $P_b \to P_c$ and $P_b \to P_c^*$ decays, with P_b and P_c pseudoscalar mesons ($\bar{B}_c$ or $\bar{B}$ and η_c or D, respectively) and P_c^* a vector meson (J/ψ or D^*).

For the case of $\bar{B} \to D^{(*)}$ decays, the hadronic matrix elements are relatively well known. In fact, there exists some experimental q^2-shape information [4,5], which can be used to constrain the transition form factors. They are then computed using a heavy quark effective theory parametrization that includes corrections of order α_s, $\Lambda_{\rm QCD}/m_{b,c}$ and partly $(\Lambda_{\rm QCD}/m_c)^2$ [15]. Moreover, some inputs from lattice quantum chromodynamics (LQCD) [36–39], light-cone [40] and QCD sum rules [41–43] are also available. In addition, a considerable number of phenomenological

[1] In fact, full general expressions for both LAB and c.m. decay distributions, decomposed in helicity contributions of the outgoing charged lepton, can also be found in [33].

studies [31,44–56] have already discussed some specific details of the c.m. $d^2\Gamma/(d\omega d\cos\theta_\ell)$ distribution, as for instance the τ-forward-backward and polarization asymmetries.[2] Other observables present in the full four-body $\bar{B} \to D^*(D\pi)\tau\nu_\tau$ angular distribution, and their power to distinguish between different NP scenarios, have also been addressed in Refs. [45,46,48], with the emphasis in the first two works focused on CP violating quantities, while in the latter one the possible pollution of $\bar{B} \to D^*(D\pi)_S\ell\bar{\nu}_\ell$ by the $\bar{B} \to D_0^*(2400)\ell\bar{\nu}_\ell$, with $D_0^*(2400)$ a broad isoscalar S-wave meson, is also analyzed. In Ref. [47], the $\bar{B} \to D^*(DY)\tau(X\nu_\tau)\bar{\nu}_\tau$, with $Y = \pi$ or γ and $X = \ell\bar{\nu}_\ell$ or π, reactions are studied, paying attention to interference effects in the full phase space of the visible τ and D^* decay products in the presence of NP. Such effects are missed in analyses that treat the τ or D^* or both as stable, and in addition, it is argued in [47] that analyses including more differential kinematic information can provide greater discriminating power for NP than single kinematic variables alone. The full five-body $\bar{B} \to D^*(D\pi)\tau(\pi\nu_\tau)\bar{\nu}_\tau$ angular distribution has also been analyzed in Ref. [56], where it is claimed that magnitudes and relative phases of all the NP Wilson coefficients can be extracted from a fit to this full five-body angular distribution.

In this work, with respect to the $\bar{B} \to D^{(*)}$ transitions, we have used the set of form factors and Wilson coefficients found in [31] and, in addition to the c.m. distribution, we present in Sec. III for the first time details of the LAB $d^2\Gamma/(d\omega E_\ell)$ differential decay width and its usefulness to distinguish between different NP scenarios.

The analysis of the $\bar{B}_c \to \eta_c$, J/ψ transitions is more novel, with a less abundant previous literature [25,27,57]. These works analyze NP effects on the c.m. angular distribution observables, with right-handed neutrino terms also considered in [57]. Here, in Sec. II, we discuss the relevance of NP in the $d^2\Gamma/(d\omega d\cos\theta_\ell)$ and $d^2\Gamma/(d\omega dE_\ell)$ distributions for both decays, highlighting the observables that are able to tell apart different NP fits among those preferred in [31]. We also show results with a polarized final τ lepton (Sec. II B).

As for the $\bar{B}_c \to \eta_c$ and $\bar{B}_c \to J/\psi$ hadronic matrix elements, different theoretical schemes were examined in Ref. [25]. Form factors obtained within the nonrelativistic (NRQM), the covariant light-front and the covariant confined quark models of Refs. [19,21,25] respectively, together with those derived in perturbative QCD (pQCD) [22] and the QCD and nonrelativistic QCD sum rule approaches of Refs. [58,59] were compared in [25]. On the other hand, a model independent global study of only the form factors involved in the SM matrix elements was conducted in Ref. [60]. It exploited preliminary lattice-QCD data from Ref. [61], dispersion relations and heavy-quark symmetry. Importantly, such analysis provided realistic uncertainty bands for the relevant form factors. Finally, very recently the HPQCD collaboration has reported a LQCD determination of the SM vector and axial form factors for the $\bar{B}_c \to J/\psi$ semileptonic decay [62]. These LQCD results have been used in Ref. [63] to evaluate $\mathcal{R}_{J/\psi}$ and angular distribution observables both, within the SM and including C_{V_L} and C_{V_R} NP terms. We note, however, that in order to calculate the effect of all NP terms in Eq. (3), some additional form factors, not determined in Refs. [60,62], are also needed.

In summary, there are different theoretical determinations of the form factors but, to our knowledge, there exist neither shape measurements nor systematic LQCD calculations, except for the very recent work of the HPQCD collaboration, and only for the SM vector and axial form factors of the $\bar{B}_c \to J/\psi$ decay. For our numerical calculations, we will not use the incomplete LQCD input, and we shall employ the form factors obtained within the NRQM scheme of Ref. [19]. One of the advantages of such choice is consistency, since all the form factors needed to compute the full NP effects encoded in Eq. (3) will be obtained within the same scheme, and without having to rely on quark field level equations of motion. Furthermore, the effects of NP on $\bar{B}_c \to \eta_c$ and $\bar{B}_c \to J/\psi$ decays will be consistently compared in this way, since there is no LQCD information for the $\bar{B}_c \to \eta_c$ reaction either. The form factors computed in [19] follow a pattern consistent with heavy quark spin symmetry (HQSS) and its expected breaking corrections. Moreover, five different reasonable interquark potentials were considered in [19], and the range of results obtained from them allows us to provide theoretical uncertainties to our predictions. Additionally, we shall also consider the form factors from the pQCD factorization approach of Ref. [22] that have recently been used in Refs. [23,31] to predict the $\mathcal{R}_{J/\psi}$ ratio within different NP scenarios. However, as we shall see below, these latter form factors do not respect a kinematical constraint at $q^2 = 0$ and they display large violations of HQSS.

Since SM LQCD vector and axial form factors are now available for the $\bar{B}_c \to J/\psi$ decay, we have systematically compared, both in the c.m. and LAB frames, SM observables computed with the LQCD input [62] and using the phenomenological NRQM. In general, though there appear overall normalization inconsistencies, we find quite good agreements for ω (or q^2) shapes, which become much better for observables constructed out of ratios of distributions, like the τ-forward-backward [$\mathcal{A}_{\rm FB}$] and τ-polarization [$\mathcal{A}_{\lambda_\tau}$] asymmetries, as well as the ratios between predictions obtained in τ and (e/μ) modes like $\mathcal{R}_{J/\psi}$ or $\mathcal{R}(\mathcal{A}_{\rm FB})$.

[2]Indeed, Eq. (5) for the c.m. angular distribution of the semileptonic decays of a pseudoscalar meson to a daughter pseudoscalar or vector meson is well known. The coefficient functions are commonly given in terms of the mediator helicity amplitudes, and several studies propose a series of quantities to check for the presence of NP, see for instance Ref. [48].

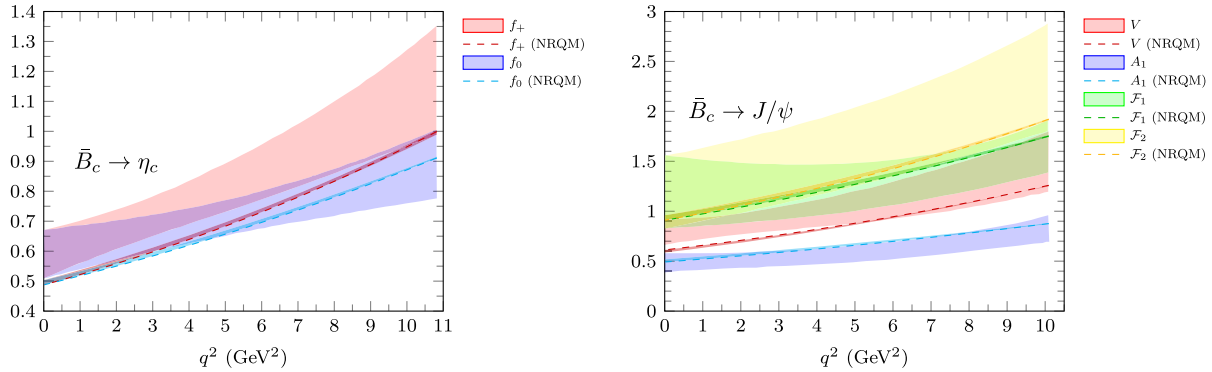

FIG. 1. Comparison of the SM form factors for the $\bar{B}_c \to \eta_c$ (left) and $\bar{B}_c \to J/\psi$ (right) transitions, obtained with the NRQM calculation of Ref. [19] (dashed lines plus narrow uncertainty bands around them) and in the model independent analysis carried out in Ref. [60] (shown as bands). For a definition of the depicted form factors see Eqs. (2), (3), and (7)–(9) of Ref. [60]. As in Figs. 6 and 7 of this latter reference, the dimension-full f_0 and $\mathcal{F}_1$ form factors are given in units of $(M^2 - M'^2)$ and $\frac{1}{2}(M^2 - M'^2)$, respectively.

This work is organized as follows: in Sec. II we present the results for the $\bar{B}_c \to \eta_c$, J/ψ semileptonic decays both for unpolarized and polarized (well-defined helicity in the c.m. or LAB frames) final τ's. The corresponding results for the $\bar{B} \to D^{(*)}$ reactions are given in Sec. III for the unpolarized cases, and in the Appendix D for the decays with polarized outgoing leptons. We find that the qualitative characteristics of the observables and the main extracted conclusions are similar to those discussed for the $\bar{B}_c \to \eta_c, J/\psi$ transitions. The most relevant findings of this work are summarized in Sec. IV. Besides, the definition of the form factors appropriate for these processes is given in Appendix A, while the expressions for the 16 $\tilde{W}$ SFs in terms of the form factors and Wilson coefficients are compiled in Appendixes B 1 and B 2 for decays into pseudoscalar and vector mesons, respectively. Finally, in Appendix C we collect the expressions for the $\bar{B}_c \to \eta_c$ and $\bar{B}_c \to J/\psi$ semileptonic decay form factors obtained within the NRQM of Ref. [19].

II. $\bar{B}_c \to \eta_c$ AND $\bar{B}_c \to J/\psi$ SEMILEPTONIC DECAY RESULTS

In this section we present the results for the $\bar{B}_c \to \eta_c \tau \bar{\nu}_\tau$ and $\bar{B}_c \to J/\psi \tau \bar{\nu}_\tau$ semileptonic decays. For the NP terms we use the Wilson coefficients corresponding to fits 6 and 7 in Ref. [31]. Among the different scenarios studied in that reference, only fits 4–7 include all the NP terms in Eq. (3). However, fits 4 and 5 lead to an unlikely physical situation in which the SM coefficient is almost canceled and its effect is replaced by NP contributions. The numerical values of the Wilson coefficients (fitted parameters) are compiled in Table VI of Ref. [31]. The data used for the fits include the $\mathcal{R}_D$ and $\mathcal{R}_{D^*}$ ratios, the normalized experimental distributions of $d\Gamma(\bar{B} \to D\tau\bar{\nu}_\tau)/dq^2$ and $d\Gamma(\bar{B} \to D^*\tau\bar{\nu}_\tau)/dq^2$ measured by Belle and *BABAR* as well as the longitudinal polarization fraction $F_L^{D^*} = \Gamma_{\lambda_{D^*}=0}(\bar{B} \to D^*\tau\bar{\nu}_\tau)/\Gamma(\bar{B} \to D^*\tau\bar{\nu}_\tau)$ provided by Belle. The χ^2 merit function is defined in Eq. (3.1) of Ref. [31], and it is constructed with the above data inputs and some prior knowledge of the $\bar{B} \to D$ and $\bar{B} \to D^*$ semileptonic form factors. Some upper bounds on the leptonic decay rate $\bar{B}_c \to \tau\bar{\nu}_\tau$ are also imposed. The corresponding $\chi^2_{\rm min}$/d.o.f. are 37.6/53 and 38.9/53 for fits 6 and 7 respectively.

As already mentioned, for the form factors, defined in Appendix A, we shall use two different sets obtained within two independent theoretical approaches.

The first one is determined from the NRQM calculations of Ref. [19]. There, five different interquark potentials are used: AL1, AL2, AP1 and AP2 taken from Refs. [64,65], and the BHAD potential from Ref. [66]. All the form factors are obtained without the need to rely on quark field level equations of motion and their expressions in terms of the quark wave functions can be found in Appendix C. As in Ref. [19], we will take as central values of the computed quantities the results corresponding to the AL1 potential. The deviations from this result obtained with the other four potentials are used to estimate the theoretical error associated to the form-factors determination in this type of models. These errors will be shown in the corresponding figures below as uncertainty bands.

A comparison of the SM form factors thus obtained with the ones from Ref. [60] is presented in Fig. 1. We see that NRQM results comfortably lie, best for the J/ψ decay and in the large q^2 region (close to zero recoil), within the colored bands which show the one-standard-deviation (1σ) best-fit regions obtained from the global dispersive analysis carried out in [60].

To evaluate the theoretical error associated to the Wilson coefficients for each of fits 6 and 7, we use different sets of coefficients obtained through successive small steps in the multiparameter space, with each step leading to a moderate χ^2 enhancement. We use 1σ sets, i.e., values of the Wilson coefficients for which $\Delta\chi^2 \leq 1$ with respect to its minimum

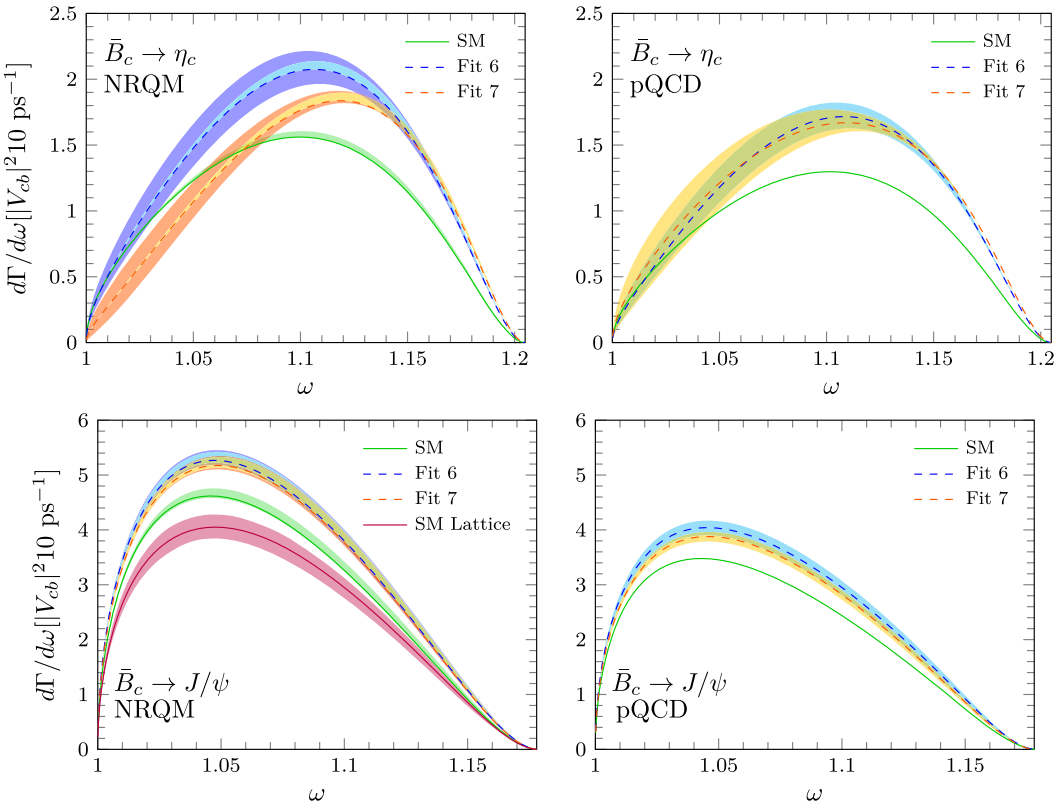

FIG. 2. Top: $d\Gamma(\bar{B}_c \to \eta_c \tau \bar{\nu}_\tau)/d\omega$ differential decay width, as a function of ω and in units of $10|V_{cb}|^2 \mathrm{ps}^{-1}$. We show SM predictions and full NP results obtained using the Wilson coefficients from fits 6 and 7 of Ref. [31] and form factors from the NRQM (left panel) and the pQCD (right panel) approaches of Refs. [19,22], respectively. Bottom: same as before but for the $\bar{B}_c \to J/\psi \tau \bar{\nu}_\tau$ decay. In the left-bottom plot, we also show the SM lattice result from Ref. [63]. Uncertainty bands are obtained as detailed in the main text.

value, to generate the distribution of each observable, taking into account in this way statistical correlations. From this derived distribution, we determine the maximum deviation above and below its central value, the latter obtained with the values of the Wilson coefficients corresponding to the minimum of χ^2 and the AL1 form factors. These deviations define the, asymmetric in general, uncertainty associated with the NP Wilson coefficients. The two types of errors are then added in quadrature and they are shown in the figures as an extra, larger in size, uncertainty band.

The second set of form factors we shall use are the ones evaluated in Ref. [22] within a perturbative QCD (pQCD) factorization approach. In this latter case only vector and axial-vector form factors have been obtained.[3] They have been evaluated in the low q^2 region and extrapolated to higher q^2 values using a model dependent parametrization. These form factors have been used in the two recent calculations of Refs. [23,31] where the rest of the form factors needed (scalar, pseudoscalar or tensor ones) were determined using the quark level equations of motion of Ref. [67]. In Ref. [22], the authors give the theoretical uncertainties for the vector and axial form factors at $q^2 = 0$. However, neither correlations nor errors for the parameters used in the q^2 extrapolation are provided. Besides, it is not clear what errors are introduced in the calculation through the use of the quark level equations of motion. Thus, in this case we will only show the error band stemming from the Wilson coefficients, even though larger uncertainties are to be expected.

As mentioned, for the $\bar{B}_c \to J/\psi$ decay, we shall compare our SM results with the ones reported in Ref. [63], and obtained with the LQCD axial and vector form factors determined in Ref. [62]. In this case the 1σ uncertainty bands are obtained with the use of the correlation matrix provided in this latter reference.

A. Results with an unpolarized final τ lepton

We begin with the results corresponding to an unpolarized final τ lepton. In Fig. 2, we show the $d\Gamma/d\omega$ differential distribution for $\bar{B}_c \to \eta_c \tau \bar{\nu}_\tau$ and $\bar{B}_c \to J/\psi \tau \bar{\nu}_\tau$ reactions. As can be seen in the plots, the ω values accessible in the transitions are around $\omega \sim 1.2$ at most,

[3]Note that in Ref. [22] they work with different form factor decompositions than those used here. The relations between our form factors and theirs can be obtained straightforwardly.

TABLE I. $\mathcal{R}_{\eta_c}$ and $\mathcal{R}_{J/\psi}$ ratios obtained in the SM and with NP effects from Ref. [31]. We give results using the [NRQM] [19] and [pQCD] [22] sets of form factors, and additionally $\mathcal{R}^{\rm SM}_{J/\psi}$ from the LQCD analysis carried out by the HPQCD collaboration [63].

	SM			NP fit 6		NP fit 7	
	[NRQM]	[pQCD]	[HPQCD]	[NRQM]	[pQCD]	[NRQM]	[pQCD]
$\mathcal{R}_{\eta_c} = \frac{\Gamma(\bar{B}_c \to \eta_c \tau \bar{\nu}_\tau)}{\Gamma(\bar{B}_c \to \eta_c \mu \bar{\nu}_\mu)}$	$0.349^{+0.000}_{-0.007}$	0.309		$0.452^{+0.034}_{-0.030}$	$0.40^{+0.03}_{-0.03}$	$0.384^{+0.024}_{-0.018}$	$0.40^{+0.04}_{-0.03}$
$\mathcal{R}_{J/\psi} = \frac{\Gamma(\bar{B}_c \to J/\psi \tau \bar{\nu}_\tau)}{\Gamma(\bar{B}_c \to J/\psi \mu \bar{\nu}_\mu)}$	$0.266^{+0.000}_{-0.004}$	0.289	0.2601 ± 0.0036	$0.306^{+0.007}_{-0.007}$	$0.342^{+0.013}_{-0.015}$	$0.301^{+0.005}_{-0.007}$	$0.326^{+0.008}_{-0.009}$

while for the similar $\bar{B} \to D^{(*)} \tau \bar{\nu}_\tau$ reactions the available phase space is larger, and ω varies from 1 to 1.35–1.40.

In both $\bar{B}_c$ decays, the NRQM form factors from Ref. [19] lead to larger total widths. Looking at the SM results for the $\bar{B}_c \to J/\psi$ decay, one sees that the LQCD prediction from Ref. [63] is in between the NRQM and pQCD distribution, somewhat closer to the former one, but still showing a tension of around 2σ in most of the phase space. Since relativistic effects increase[4] as one departs from zero recoil to $q^2 = 0$, they might be responsible for some of the NRQM-LQCD discrepancies exhibited in the figure far from the vicinity of $\omega = 1$.

For the decay into η_c computed with the NRQM form factors we note that already $d\Gamma/d\omega$ discriminate between NP fits 6 and 7. For the rest of the cases shown in the figure, though NP effects are clearly visible, we see that this observable would not be able to distinguish between the two NP scenarios examined in this work.

Evaluating the SM predictions for a final massless charged lepton (μ or e), we obtain the $\mathcal{R}_{\eta_c}$ and $\mathcal{R}_{J/\psi}$ ratios collected in Table I. The systematic uncertainties due to the interquark potential in the NRQM scheme are largely canceled out in the ratios, as can be inferred from the SM predictions. For the SM we find a nice agreement of the NRQM determination of $\mathcal{R}_{J/\psi}$ and the lattice evaluation of Ref. [63], pointing also to a compensation in the ratio of the overall-normalization discrepancies noted in Fig. 2. On the other hand, predictions with the NRQM and pQCD form factors differ by approximately 10%, except for NP fit 7 $\mathcal{R}_{\eta_c}$, where the change is only of 4%. In fact, the form-factor systematic uncertainties are reduced compared to those observed in some regions of the differential distributions in Fig. 2. We also note that the NRQM $\mathcal{R}_{\eta_c}$ and $\mathcal{R}_{J/\psi}$ ratios are systematically bigger and smaller, respectively, than those obtained with pQCD form factors. For the latter ratio, we mentioned above that $\Gamma^{\rm NRQM}(\bar{B}_c \to J/\psi \tau \bar{\nu}_\tau) \geq \Gamma^{\rm pQCD}(\bar{B}_c \to J/\psi \tau \bar{\nu}_\tau)$ and thus, the massless lepton modes of the $\bar{B}_c \to J/\psi$ semileptonic decay calculated with NRQM form factors must also be larger than when pQCD form factors are used. Moreover, the difference has to be greater than for the τ mode to explain $R^{\rm NRQM}_{J/\psi} \leq R^{\rm pQCD}_{J/\psi}$.

The ratios including NP are greater than pure SM expectations, around 30% and 15% for $\mathcal{R}_{\eta_c}$ and $\mathcal{R}_{J\psi}$, respectively, except for the NRQM $\mathcal{R}_{\eta_c}$ case evaluated with the NP fit 7 where an increase of only 10% is found. In fact, at the level of ratios, only the NRQM $\mathcal{R}_{\eta_c}$ discriminates between NP fits 6 and 7. One can compare the values for $\mathcal{R}_{J/\psi}$ with the only available experimental measurement quoted above. In this case we see all predictions fall short of the present central experimental value by almost 2σ, adding in quadrature the errors given in Eq. (2). The agreement is slightly better when using the pQCD form-factor set. The improvement is not significant, however, within the present accuracy in the data and, as we explain below, there are some inconsistencies in the corresponding pQCD form factors for this decay.

Now we discuss results for the $d^2\Gamma/(d\omega d\cos\theta_\ell)$ and $d^2\Gamma/(d\omega dE_\ell)$ double differential distributions. The $a_{0,1,2}$ c.m. angular and $c_{0,1,2}$ LAB energy expansion coefficients are shown in Figs. 3 and 4, and Figs. 5 and 6 for the η_c and J/ψ decay modes, respectively.

For the $\bar{B}_c \to \eta_c \tau \bar{\nu}_\tau$ decay, both sets of form factors lead to qualitatively very similar results. As in Ref. [33] for the $\Lambda_b \to \Lambda_c \tau \bar{\nu}_\tau$ semileptonic decay, we find that, with the exception of a_0, all the other expansion coefficients serve the purpose of giving a clear distinction between NP fits 6 and 7. Thus, different fits that otherwise give similar $d\Gamma/d\omega$ decay widths can be told apart by looking at these c.m. angular or LAB energy observables. In addition, we also observe ω shapes for all $\bar{B}_c \to \eta_c$ SM and NP coefficients similar to those obtained in Ref. [33] for the $\Lambda_b \to \Lambda_c$ transition, except a_0 that here grows with ω while for the baryon decay it is a decreasing function of ω.

The corresponding results for a decay into J/ψ are shown in Figs. 5 and 6. There are two distinct features in this case. First, the utility of these observables to distinguish between fits 6 and 7 and, in some cases, between those NP predictions and the SM results, is not as good as in the η_c case. This happens to be true independent of the form-factor set used. Second, the results obtained with the two form-factor sets turn out to be very different in most cases, with only a_0 and a_1 showing a similar qualitative

[4]The kinematical treatment is fully relativistic, but close to $q^2 = 0$, the transition matrix elements are sensitive to large momentum components of the nonrelativistic meson wave functions.

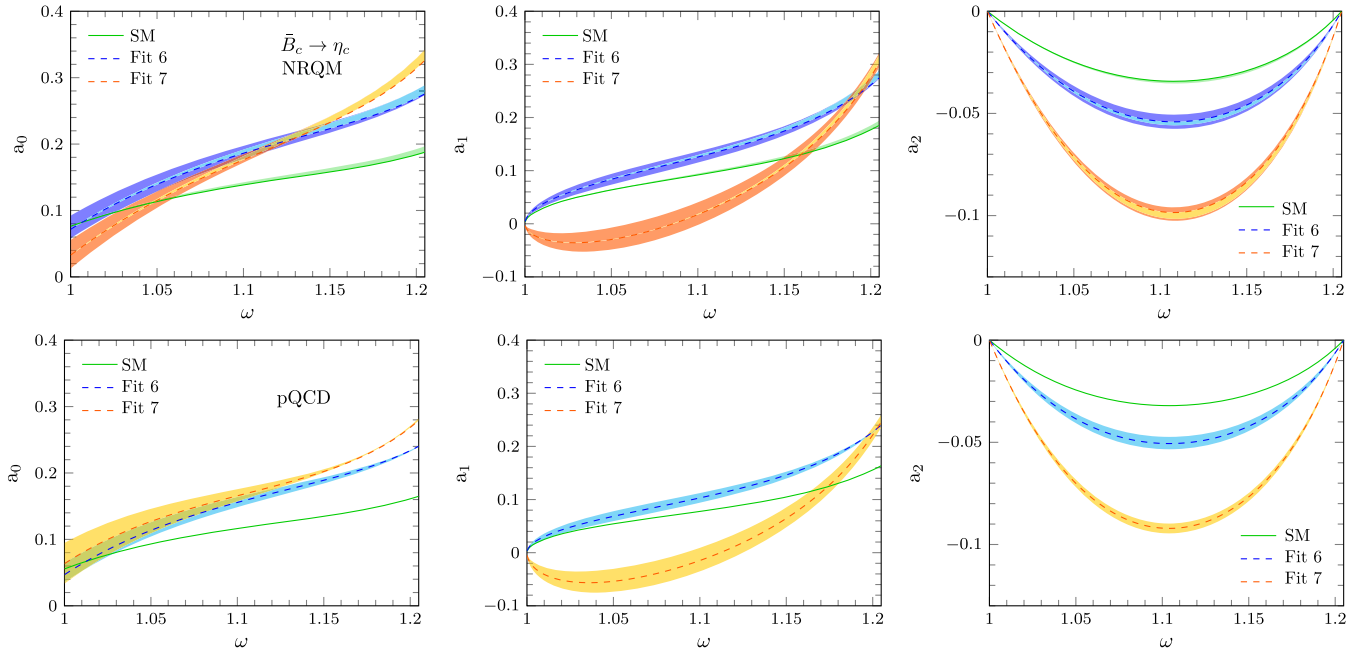

FIG. 3. $\bar{B}_c \to \eta_c \tau \bar{\nu}_\tau$ decay: c.m. $a_{0,1,2}$ angular expansion coefficients as a function of ω. We show results obtained with both NRQM (upper panels) and pQCD (lower panels) form factors from Refs. [19,22], respectively. The beyond the SM scenarios fits 6 and 7 are taken from Ref. [31]. Uncertainty bands are as in Fig. 2.

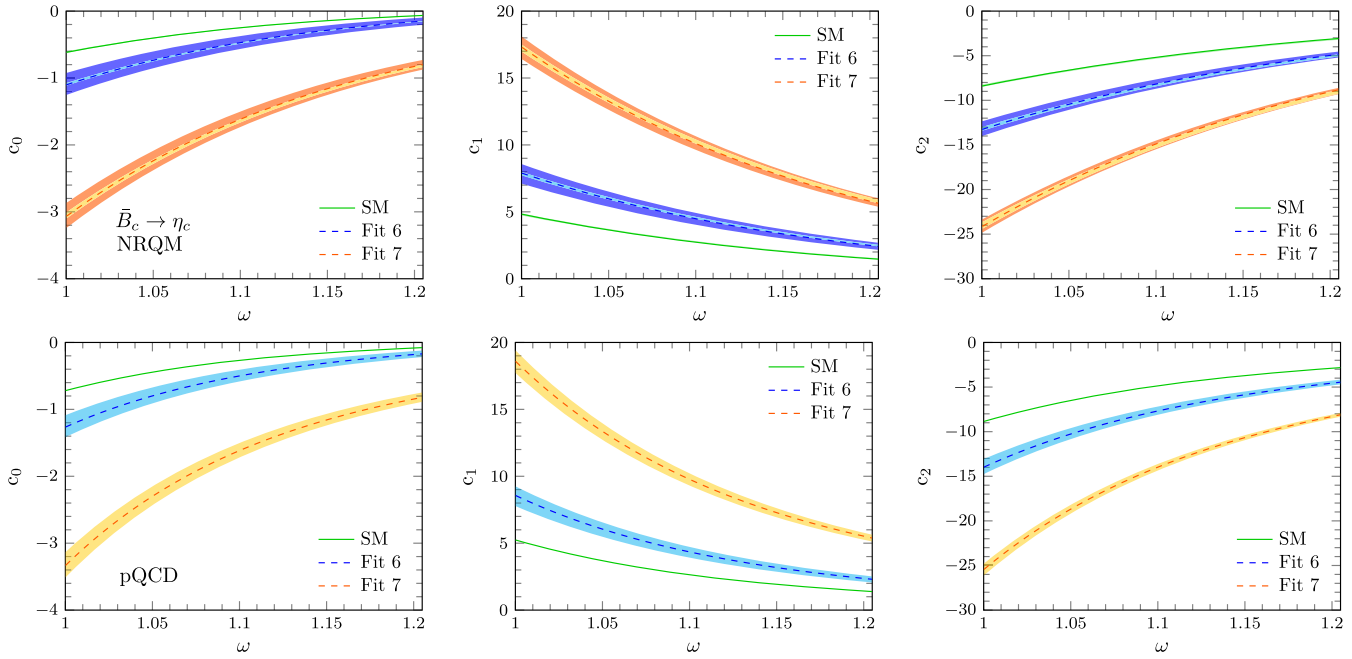

FIG. 4. $\bar{B}_c \to \eta_c \tau \bar{\nu}_\tau$ decay: Same as in Fig. 3 but for the LAB $c_{0,1,2}$ energy expansion coefficients.

behavior. By looking at SM results alone we find a good qualitative agreement between NRQM and LQCD results while, with the exception of a_0 and a_1, we find very different shapes for the results obtained using the pQCD form factors. In order to better understand this discrepancy, we show in Fig. 7 all the form factors defined in Eqs. (A1) and (A2), for decays into both η_c and J/ψ. In the left panel we give the results obtained with the AL1 NRQM of Ref. [19]. We see the results are close to expectations from Eq. (A7) based on HQSS. In the middle panel we give the results obtained using the form factors from Ref. [22] and the quark level equations of motion from Ref. [67]. Large

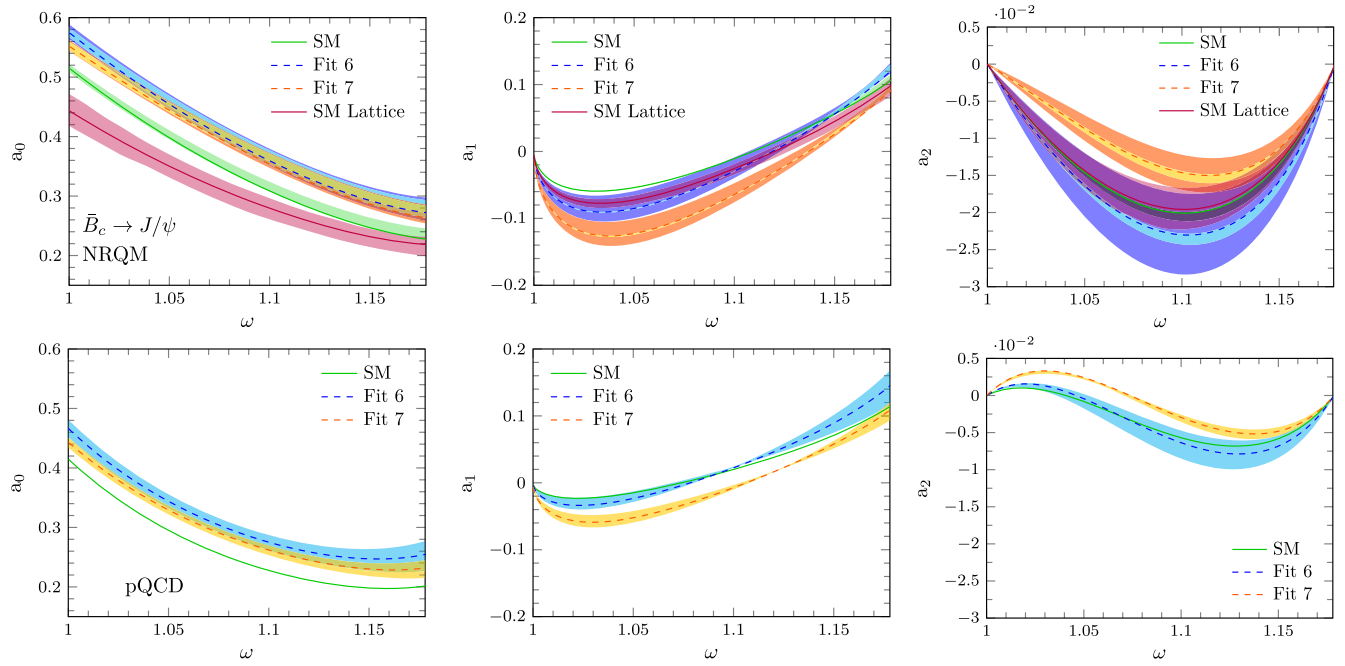

FIG. 5. $\bar{B}_c \to J/\psi\tau\bar{\nu}_\tau$ decay: c.m. $a_{0,1,2}$ angular expansion coefficients as a function of ω. We show results obtained with both, NRQM (upper panels) and pQCD (lower panels) form factors from Refs. [19,22], respectively. In the upper panels, SM results for these observables obtained with the LQCD form factors reported in Ref. [62] are also displayed. The beyond the SM scenarios fits 6 and 7 are taken from Ref. [31]. Uncertainty bands are as in Fig. 2.

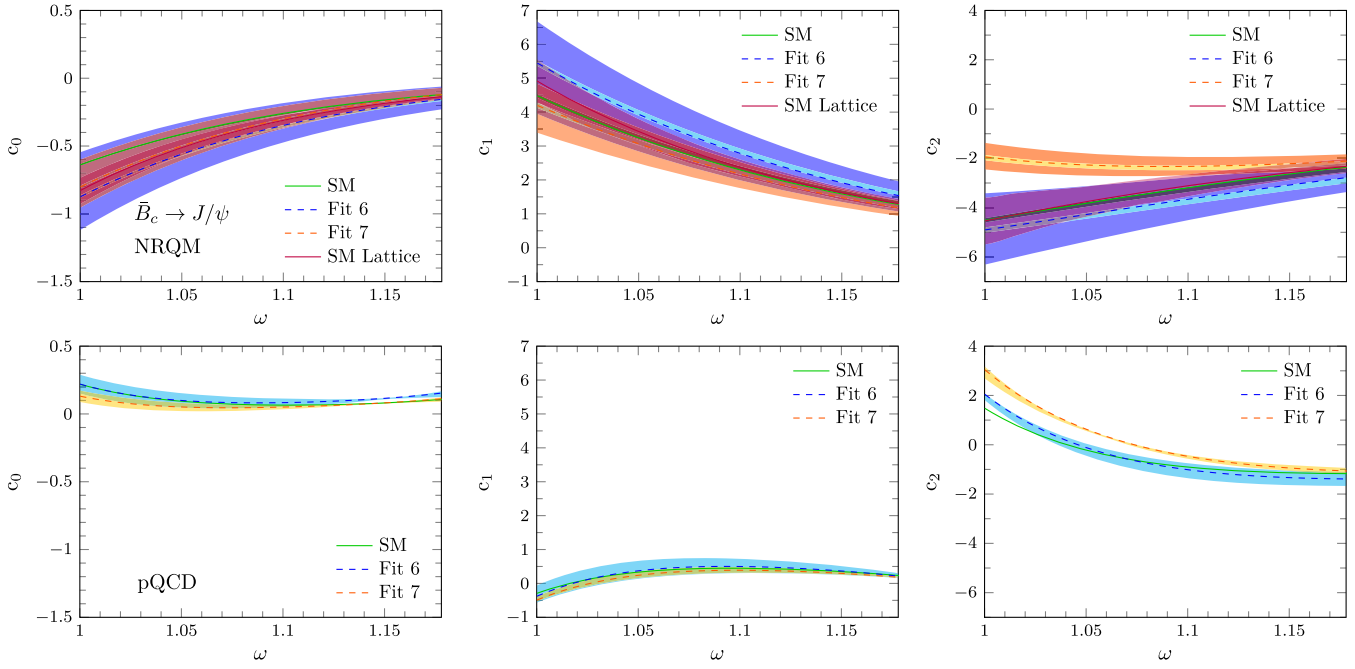

FIG. 6. $\bar{B}_c \to J/\psi\tau\bar{\nu}_\tau$ decay: Same as in Fig. 5 but for the LAB $c_{0,1,2}$ energy expansion coefficients.

violations of HQSS are already seen for h_{A_2} and h_{A_3} (where no quark level equations of motion are involved), also for h_{T_3} and, to a lesser extent, for h_P. These HQSS violations are related, at least in part, to the fact that the $A_0(q^2)$, $A_1(q^2)$ and $A_2(q^2)$ axial form factors evaluated in Ref. [22], and in terms of which the $h_{A_{1,2,3}}$ ones are determined, do not respect the $q^2 = 0$ constraint,

$$A_0(0) = \frac{M + M'}{2M'} A_1(0) - \frac{M - M'}{2M'} A_2(0). \tag{7}$$

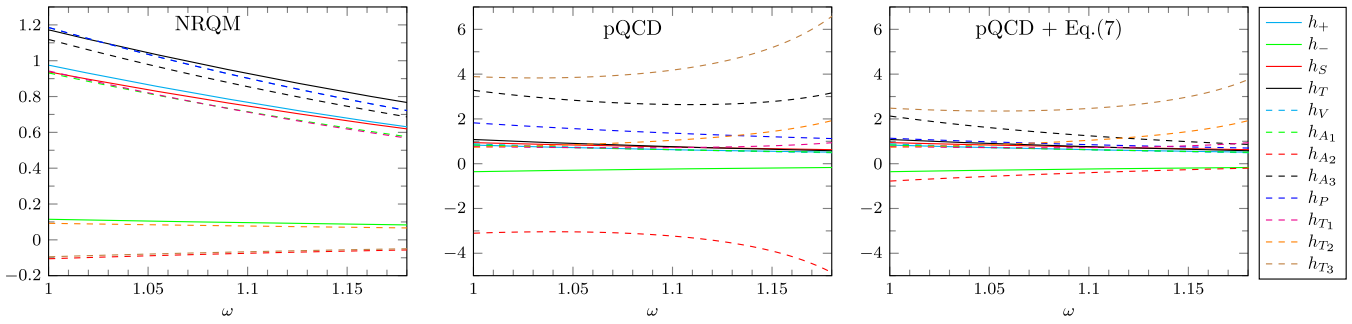

FIG. 7. Different h_a form factors defined in Eqs. (A1) and (A2) for $\bar{B}_c \to \eta_c$ and $\bar{B}_c \to J/\psi$ semileptonic decays. Left panel: results obtained with the NRQM of Ref. [19] using the AL1 potential. Middle panel: results obtained from the form factors of Ref. [22] and the use of quark-level equations of motion from Ref. [67]. Right panel: same as the middle panel but forcing Eq. (7) on $A_0(0)$.

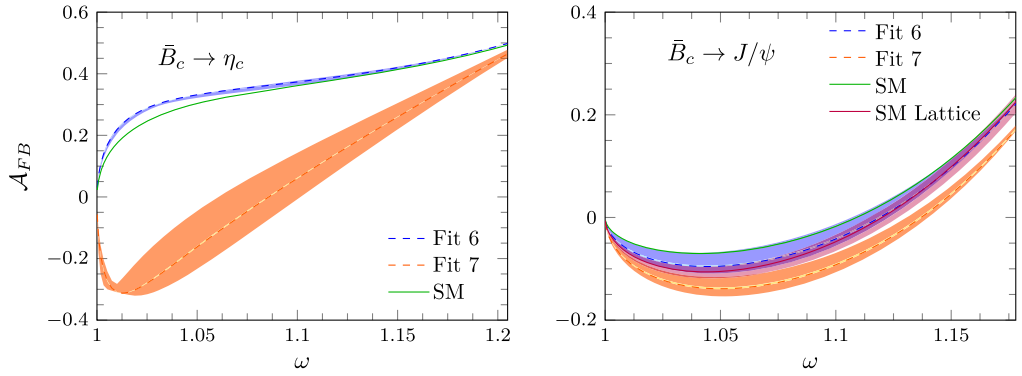

FIG. 8. Forward-backward asymmetry in the c.m. reference frame for the $\bar{B}_c \to \eta_c \tau \bar{\nu}_\tau$ (left) and $\bar{B}_c \to J/\psi \tau \bar{\nu}_\tau$ (right) decays. The results have been obtained with the form factors evaluated with the NRQM of Ref. [19]. For the $\bar{B}_c \to J/\psi$ case, we also show the SM prediction from the LQCD results of Ref. [63]. Uncertainty bands are as in Fig. 2.

Even though $q^2 \geq m_\tau^2$ for a final τ, taking the wrong values of the form factors at $q^2 = 0$ affects the determination of the values at larger q^2. In the right panel of Fig. 7 we see the effect of imposing the above constraint on $A_0(0)$. The h_P form factor is now in agreement with HQSS expectations and things improve for h_{A_2}, h_{A_3} and h_{T_3}. Note that this restriction also corrects the divergences at $q^2 = 0$ that otherwise appear for h_{A_2} and h_{A_3} which signatures are clearly visible in the middle panel at large recoils.[5] Moreover, with this restriction imposed, the results for $\mathcal{R}_{J/\psi}$ would get smaller, $0.311^{+0.007}_{-0.006}$ for fit 6 and $0.303^{+0.005}_{-0.004}$ for fit 7, and in much better agreement with the ones obtained using the NRQM form factors from Ref. [19] (see Table I). Besides, and though they are less important numerically, there are divergences in all three $h_{T_{1,2,3}}$ form factors at $q^2 = 0$ when quark-level equations of motion are used to obtain them. The beginning of these divergences can already be seen in the middle and right panels of Fig. 7.

[5]Note that when we use the form factors from Ref. [22], we determine $h_{A_{1,2,3}}$ from $A_{0,1,2}$ and the relation in Eq. (7) has to be satisfied in order for $h_{A_{2,3}}$ not to diverge at $q^2 = 0$.

In Fig. 8 we now show the forward-backward asymmetry in the c.m. frame evaluated with the form factors from the NRQM of Ref. [19]. This asymmetry is given by the ratio

$$\mathcal{A}_{\rm FB} = \frac{a_1(\omega)}{2a_0(\omega) + 2a_2(\omega)/3}. \tag{8}$$

For the decay into J/ψ, SM results for this asymmetry from the LQCD form factors of Ref. [62] are also shown. Note that $\mathcal{A}_{\rm FB}$ is given in [63] as well. For this decay mode, as it is also the case for other observables, the SM result falls into the error band of fit 6. However, for both $\bar{B}_c \to \eta_c$ and $\bar{B}_c \to J/\psi$ transitions, this observable is also able to distinguish between fits 6 and 7, in particular for the η_c channel.

B. Results with a polarized final τ lepton

In this section we collect the results corresponding to the $\bar{B}_c \to \eta_c \tau \bar{\nu}_\tau$ and $\bar{B}_c \to J/\psi \tau \bar{\nu}_\tau$ decays with a polarized τ (well-defined helicity $h = \pm 1$ in the c.m. or LAB frames). In this case, and for simplicity, we will only present results obtained with the use of the NRQM form factors from Ref. [19], and, for the $\bar{B}_c \to J/\psi$ case, also the SM results

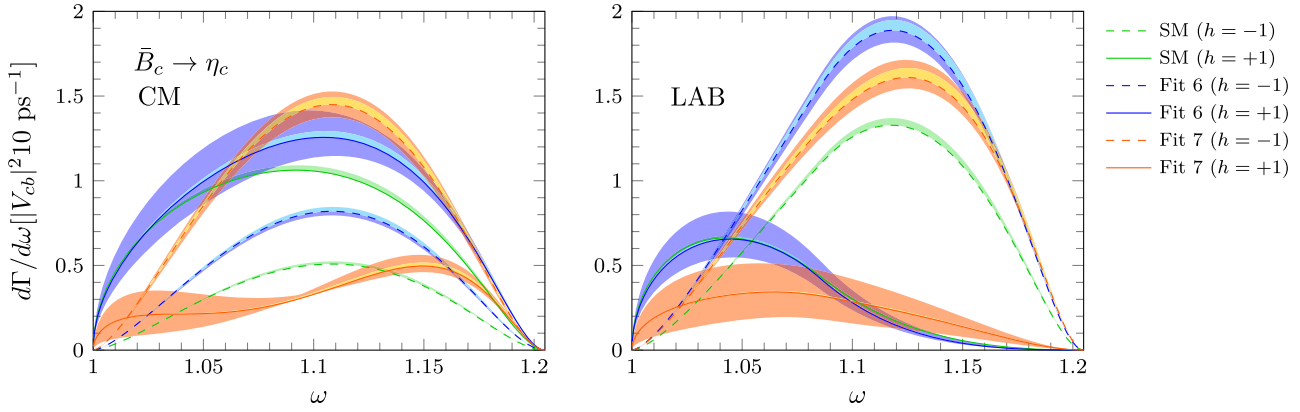

FIG. 9. c.m. (left) and LAB (right) helicity decomposition of the $d\Gamma(\bar{B}_c \to \eta_c \tau \bar{\nu}_\tau)/d\omega$ differential decay width, calculated with the NRQM form factors from Ref. [19]. Uncertainty bands are as in Fig. 2.

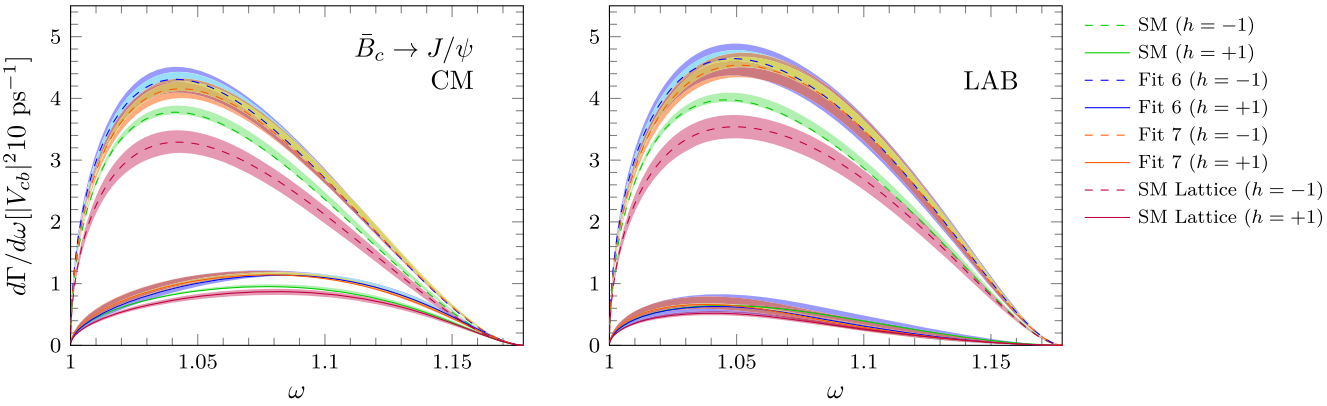

FIG. 10. As in Fig. 9, but for the $\bar{B}_c \to J/\psi \tau \bar{\nu}_\tau$ decay. We also show the SM results obtained with LQCD form factors from Ref. [62].

obtained with the LQCD form factors from Ref. [62]. In Fig. 9 we show the $d\Gamma/d\omega$ differential decay width for the $\bar{B}_c \to \eta_c \tau \bar{\nu}_\tau$ decay with a final τ with well-defined helicity in the c.m. reference frame (left panel) and in the LAB system (right panel). The corresponding results for the $\bar{B}_c \to J/\psi \tau \bar{\nu}_\tau$ decay are presented in Fig. 10. The negative helicity contribution is dominant in all cases except for the η_c c.m. distributions obtained both in the SM and in fit 6. This unexpected feature also occurs for the polarized $\bar{B} \to D \tau \bar{\nu}_\tau$ decay (see Appendix D). We see that both c.m. and LAB τ negative-helicity distributions obtained in η_c decays clearly discriminate between SM and different NP scenarios. On the other hand, for the $\bar{B}_c \to J/\psi \tau \bar{\nu}_\tau$ decay $d\Gamma/d\omega$ is not an efficient tool for that purpose, even taking into account information on the outgoing τ polarization. As we noted in Fig. 2 for the unpolarized $d\Gamma/d\omega$, the LQCD results [62] for the SM τ negative-helicity c.m. and LAB $\bar{B}_c$ distributions are around 2σ below the NRQM predictions, while the shapes turn out to be in excellent agreement.

As shown in Ref. [33], for a polarized final τ lepton with well-defined helicity $h = \pm 1$, the c.m. angular and LAB energy distributions are respectively determined by

$$\frac{2\bar{\sum}|\mathcal{M}|^2}{M^2(1-\frac{m_\ell^2}{q^2})} = a_0(\omega,h) + a_1(\omega,h)\cos\theta_\ell + a_2(\omega,h)(\cos\theta_\ell)^2 \tag{9}$$

$$\frac{2\bar{\sum}|\mathcal{M}|^2}{M^2} = \frac{1}{2}\left(c_0 + c_1\frac{E_\ell}{M} + c_2\frac{E_\ell^2}{M^2}\right) - \frac{h}{2}\frac{M}{p_\ell}\left(\hat{c}_0 + [c_0+\hat{c}_1]\frac{E_\ell}{M} + [c_1+\hat{c}_2]\frac{E_\ell^2}{M^2} + [c_2+\hat{c}_3]\frac{E_\ell^3}{M^3}\right). \tag{10}$$

In the latter equation, p_ℓ is the modulus of the final charged lepton three-momentum measured in the LAB frame. The general expressions of the $a_{0,1,2}(\omega,h)$ and $\hat{c}_{0,1,2,3}(\omega)$ coefficients in terms of the $\tilde{W}$ SFs can be found in Ref. [33]. In Figs. 11 and 12 we present the results for the functions $a_{0,1,2}(\omega, h=\pm 1)$ (c.m.) and $\hat{c}_{0,1,2,3}(\omega)$ (LAB) for the polarized $\bar{B}_c \to \eta_c \tau \bar{\nu}_\tau$ reaction.

We see that even taking uncertainties into account, fits 6 and 7 provide distinct predictions for all nonzero angular coefficients that also differ from the SM results, with the

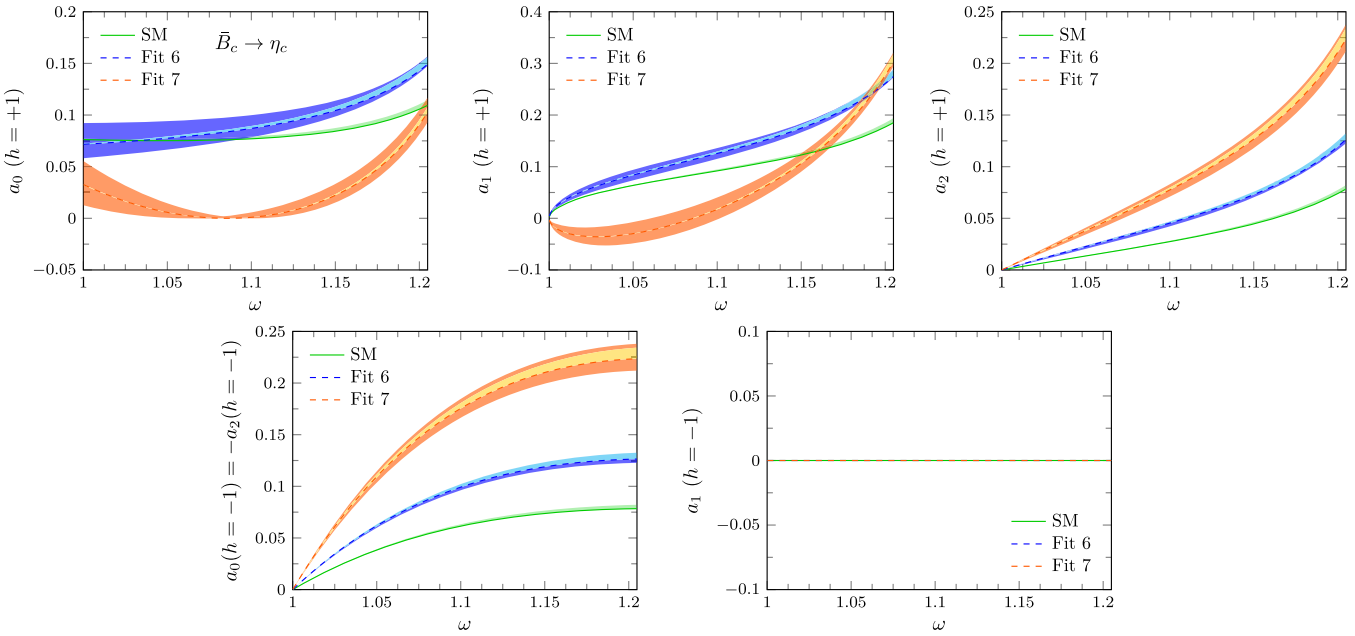

FIG. 11. c.m. angular expansion coefficients for the $\bar{B}_c \to \eta_c \tau \bar{\nu}_\tau$ decay with a polarized τ with positive (upper panels) and negative (lower panels) helicity. They have been evaluated with the NRQM form factors from Ref. [19]. Uncertainty bands as in Fig. 2.

exception of $a_0(\omega, h = +1)$, for which SM and NP fit 6 results overlap below $\omega \leq 1.1$. We also observe that for this decay ($\bar{B}_c \to \eta_c$), the relations

$$a_0(\omega, h=-1) = -a_2(\omega, h=-1), \quad a_1(\omega, h=-1) = 0 \quad (11)$$

are satisfied because of angular momentum conservation. Since both the initial and final hadrons have zero spin, the virtual particle exchanged (a W boson in the SM) should have helicity zero. In the c.m. system this corresponds to a zero spin projection along the quantization axis defined by its three-momentum in the LAB frame, the same axis that is defined by the final hadron LAB (or c.m.) three-momentum. Thus, in the c.m. system, the angular momentum of the final lepton pair measured along that axis must be zero.

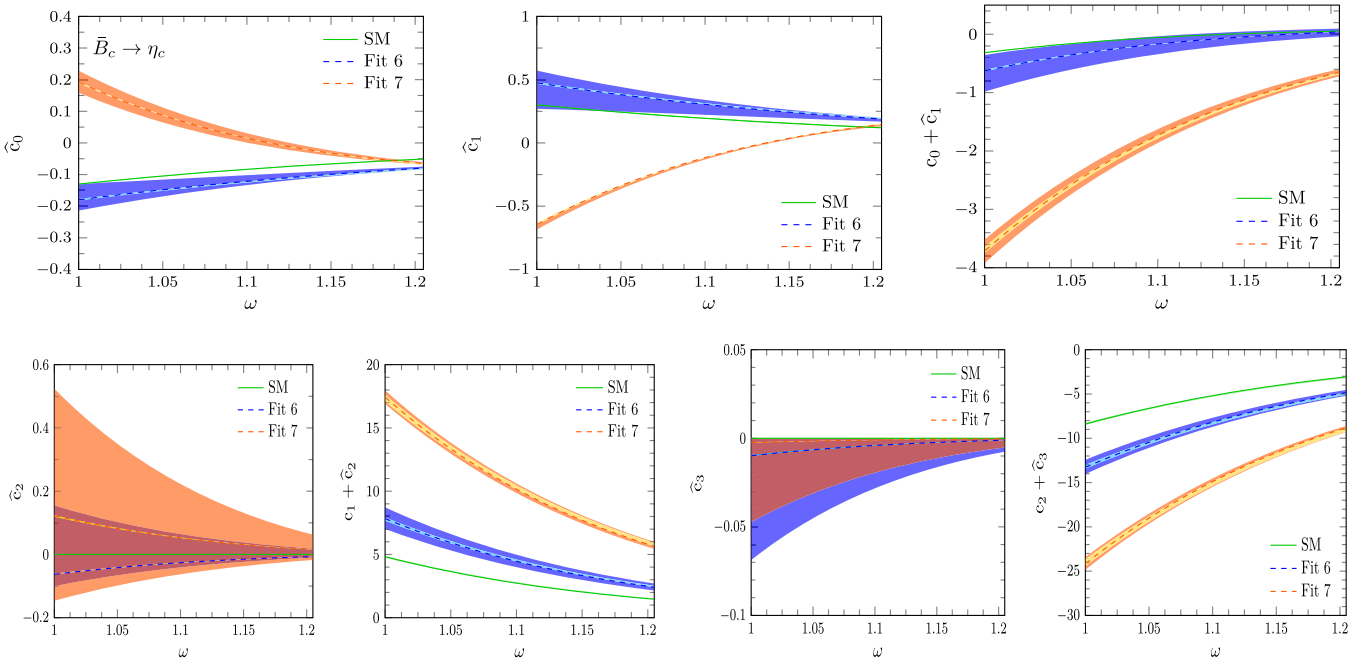

FIG. 12. LAB charged lepton energy expansion coefficients $\hat{c}_{0,1,2,3}(\omega)$ for the polarized $\bar{B}_c \to \eta_c \tau \bar{\nu}_\tau$ decay. We also show the $(c_0 + \hat{c}_1)$, $(c_1 + \hat{c}_2)$ and $(c_2 + \hat{c}_3)$ sums in the third top, second and fourth bottom panels, respectively. All the functions have been evaluated with the NRQM form factors from Ref. [19]. Uncertainty bands are as in Fig. 2.

As a consequence, the c.m. helicity of a final τ lepton emitted along that direction, which corresponds to either $\theta_\ell = 0$ or $\theta_\ell = \pi$, must equal that of the $\bar{\nu}_\tau$, the latter being always positive. This means that a negative helicity τ cannot be emitted in the c.m. system when $\theta_\ell = 0$ or π. Looking at Eq. (9), this implies that $a_0(\omega, h = -1) = -a_2(\omega, h = -1)$ and $a_1(\omega, h = -1) = 0$.

Besides, at zero recoil c.m. and LAB frames coincide and angular momentum conservation requires the helicity of the τ lepton to equal that of the antineutrino. This implies $a_0(\omega = 1, h = -1) = -a_2(\omega = 1, h = -1) = 0$, and also the cancellation of Eq. (10) at zero recoil for $h = -1$. In fact, the LAB $d^2\Gamma(\bar{B}_c \to \eta_c \tau \bar{\nu}_\tau)/(d\omega dE_\ell)$ distribution should cancel for $h = -1$ and any value of ω when E_ℓ equals its maximum value[6] for that particular ω. The reason is that this maximum E_ℓ value corresponds necessarily to $\theta_\ell = \pi$ and in that case the helicity of the τ is the same in both c.m. and LAB frames. Since $h = -1$ is forbidden in the c.m. for that specific kinematics it is also forbidden in the LAB. Note that any violation of these results will require negative helicity antineutrinos which means NP contributions with right-handed neutrinos. The possible role of such beyond the SM terms in the explanation of the LFU ratio anomalies has been considered in Refs. [47,68–77] and their existence has not been discarded by the available $\bar{B} \to D^{(*)}$ data [78].

Note also that, as a result of $a_1(\omega, h = -1)$ being zero for the $P_b \to P_c$ decays, the forward-backward asymmetry in the c.m. system ($\mathcal{A}_{\rm FB}$ shown in the left panel of Fig. 8) can only originate from positive helicity τ's. For the same reason, for massless charged leptons ($\ell = e, \mu$), $\mathcal{A}_{\rm FB}$ vanishes in the SM for transitions between pseudoscalar mesons.

Looking at positive helicities, one finds that, in the high ω region, the quantity $a_0(\omega, h = +1) - a_1(\omega, h = +1) + a_2(\omega, h = +1)$ shows a steady decrease, as ω increases. In fact, at maximum recoil, one has the approximate result:

$$a_0(\omega_{\rm max}, h = +1) - a_1(\omega_{\rm max}, h = +1) + a_2(\omega_{\rm max}, h = +1) \approx 0, \tag{13}$$

which can be readily inferred from the corresponding figures and which corresponds to a very small probability of c.m. positive helicity τ's emitted at $\theta_\ell = \pi$ when $\omega = \omega_{\rm max}$. This result can be partially understood taking into account that our main contribution selects negative chirality for the final charged lepton.[7] A τ lepton emitted with positive helicity in the c.m. frame and with $\theta_\ell = \pi$ will also have positive helicity in the LAB frame. However, close to maximum recoil its momentum in the LAB is very large and helicity almost equals chirality, hence the partial cancellation. Note that this result would be independent of the spin of the hadrons involved as long as negative chirality lepton current operators are dominant. This approximate relation in Eq. (13) can already be seen in the polarized results for the $\Lambda_b \to \Lambda_c$ decay shown in Ref. [33]. Besides, and for the same chirality/helicity argument, one expects the LAB ratio $\frac{d\Gamma/d\omega(h=+1)}{d\Gamma/d\omega(h=-1)}$ to be small in the high ω region, the reason being that for ω close to $\omega_{\rm max}$ the charged lepton energies are significantly larger than its mass.

In Fig. 12 we present the results for the $\hat{c}_{0,1,2,3}(\omega)$ coefficients associated to this decay. We observe that $\hat{c}_0(\omega)$ and $\hat{c}_1(\omega)$ are able to distinguish between the two NP fits from Ref. [31] considered in the present work. The other two observables $\hat{c}_2(\omega)$ and $\hat{c}_3(\omega)$, available from the polarized $d^2\Gamma(\bar{B}_c \to \eta_c \tau \bar{\nu}_\tau)/(d\omega dE_\ell)$ distribution, turn out to be very small and negligible when compared with c_1 and c_2, respectively (see the plots in Fig. 12). Therefore, these two additional coefficients have little relevance in the discussion of the NP fits 6 and 7, for which the NP tensor Wilson coefficient $|C_T| \sim 10^{-2}$ is quite small. As discussed in Ref. [33], $\hat{c}_2$ and $\hat{c}_3$ are, however, optimal observables to restrict the validity of NP schemes with larger $|C_T|$ values.

In Figs. 13 and 14 we collect the corresponding results for the $\bar{B}_c \to J/\psi \tau \bar{\nu}_\tau$ decay. In this case, no angular momentum related restriction is in place for $a_{0,1,2}(\omega, h = -1)$ since the final hadron has spin one and there are three possible helicity states. However, one can see that the approximate relation in Eq. (13) is indeed satisfied. Also the discussion above about the LAB ratio $\frac{d\Gamma/d\omega(h=+1)}{d\Gamma/d\omega(h=-1)}$ being small near maximum recoil also applies for this decay. When looking at SM results alone we find a qualitative agreement of NRQM and LQCD results.

To conclude this section, in Fig. 15 we present the results for the τ polarization asymmetry

$$\mathcal{A}_{\lambda_\tau} = \frac{d\Gamma/d\omega(h = -1) - d\Gamma/d\omega(h = +1)}{d\Gamma/d\omega(h = -1) + d\Gamma/d\omega(h = +1)} \tag{14}$$

measured both in the c.m. and LAB frames.

For the $\bar{B}_c \to \eta_c$ decay we see that both polarization asymmetries equal minus one at zero recoil and that the LAB one tends to plus one when maximum recoil is approached. The Wilson coefficients of the charged-lepton positive chirality $\mathcal{O}_{S_L,S_R}$ operators in fit 7 are significantly larger than in fit 6, which explains the larger deviations of $\mathcal{A}_{\lambda_\tau}$ from $+1$ at $\omega = \omega_{\rm max}$ in the first NP scenario. This is in perfect accordance with the discussion above. As it is clear from the figure, the c.m. polarization asymmetry is a good observable to distinguish between different NP scenarios. This is not the case however of the LAB one. For the $\bar{B}_c \to J/\psi$ decay the asymmetries are equal at zero recoil, since c.m. and LAB frames coincide at $\omega = 1$, but otherwise they show a very different ω dependence. None of them is able to

[6]The maximum E_ℓ^+ and minimum E_ℓ^- energy values allowed to the final charged lepton for a given ω are

$$E_\ell^\pm = \frac{(M - M'\omega)(q^2 + m_\ell^2) \pm M'\sqrt{\omega^2 - 1}(q^2 - m_\ell^2)}{2q^2}. \tag{12}$$

[7]Note that only the $\mathcal{O}_{S_L,S_R}$ and $\mathcal{O}_T$ NP terms in Eqs. (3) and (4) select positive chirality for the final charged lepton.

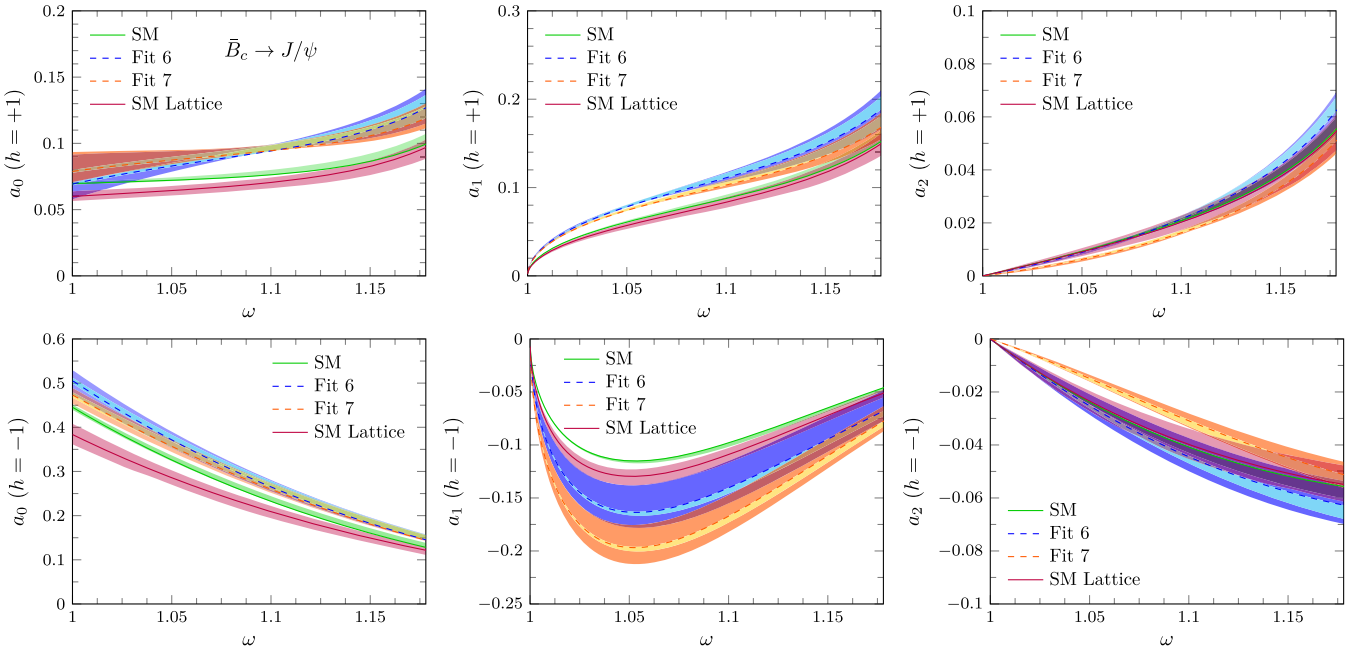

FIG. 13. c.m. angular expansion coefficients for the $\bar{B}_c \to J/\psi\tau\bar{\nu}_\tau$ decay with a τ with positive (upper panels) and negative (lower panels) helicity. They have been evaluated with the NRQM form factors from Ref. [19]. We also show the SM results obtained with LQCD form factors from Ref. [62]. Uncertainty bands are as in Fig. 2.

distinguish NP results for fits 6 and 7 among themselves and from the SM. We also observe for these latter decays, a quite good agreement between NRQM and LQCD predictions in particular for the results found in the c.m. frame, which are also reported in the recent analysis of Ref. [63].

Although the $\bar{B}_c \to J/\psi$ decay is perhaps easier to measure experimentally, as a general rule we find the $\bar{B}_c \to J/\psi$ observables, also in the case of a polarized τ, are less optimal for distinguishing between NP fits 6 and 7 than those discussed above for $\bar{B}_c \to \eta_c$ decays, or

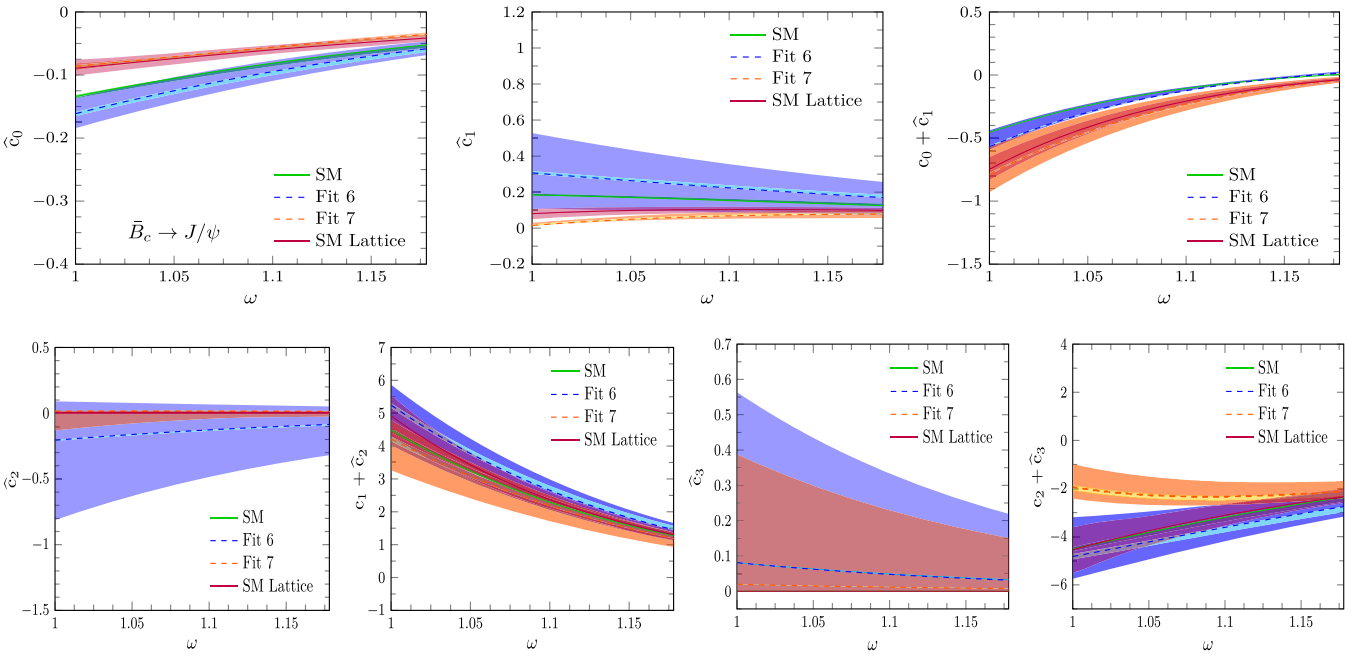

FIG. 14. LAB charged lepton energy expansion coefficients $\hat{c}_{0,1,2,3}(\omega)$ for the polarized $\bar{B}_c \to J/\psi\tau\bar{\nu}_\tau$ decay. We also show the $(c_0 + \hat{c}_1)$, $(c_1 + \hat{c}_2)$ and $(c_2 + \hat{c}_3)$ sums in the third top, second and fourth bottom panels, respectively. All the functions have been evaluated with the NRQM form factors from Ref. [19]. We also show the SM results obtained with LQCD form factors from Ref. [62]. Uncertainty bands are as in Fig. 2.

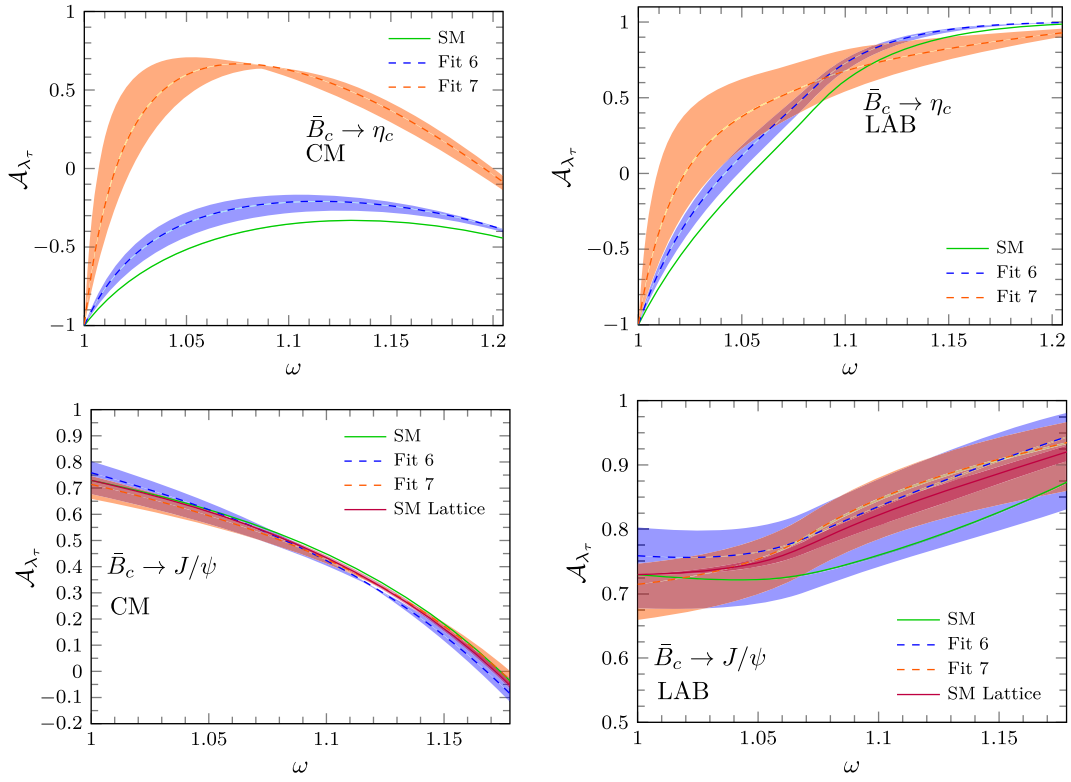

FIG. 15. τ polarization asymmetry $\mathcal{A}_{\lambda_\tau}$, defined in Eq. (14), for the $\bar{B}_c \to \eta_c$ (upper panels) and $\bar{B}_c \to J/\psi$ (lower panels) semileptonic decays measured in the c.m. (left panels) and LAB (right panels) frames. They have been obtained with the NRQM form factors from Ref. [19]. For the $\bar{B}_c \to J/\psi$ case we also show the SM results obtained with the LQCD form factors from Ref. [62]. Uncertainty bands are as in Fig. 2.

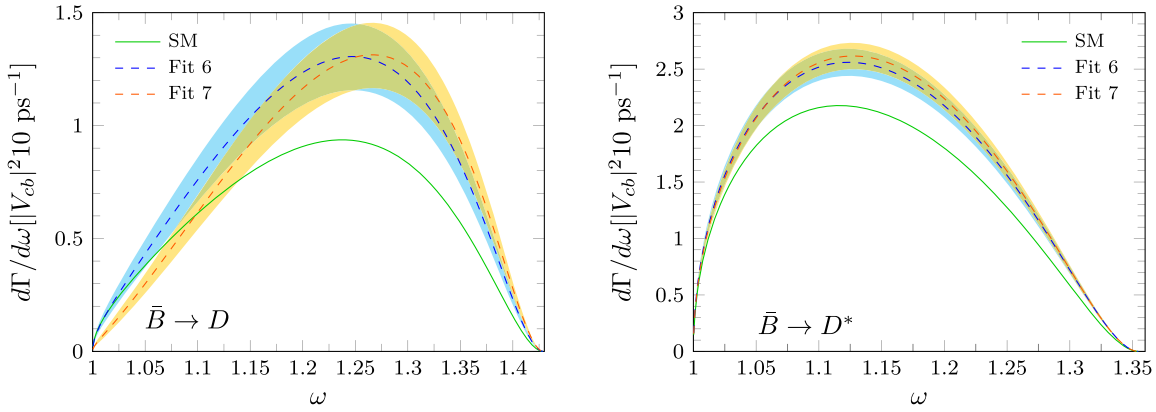

FIG. 16. $d\Gamma(\bar{B} \to D\tau\bar{\nu}_\tau)/d\omega$ (left) and $d\Gamma(\bar{B} \to D^*\tau\bar{\nu}_\tau)/d\omega$ (right) differential decay widths, as a function of ω and in units of $10|V_{cb}|^2\mathrm{ps}^{-1}$. We show SM predictions and full NP results obtained using the Wilson coefficients and form factors corresponding to fits 6 and 7 of Ref. [31]. Uncertainty bands are obtained as explained in the main text.

those presented in Ref. [33] for the related $\Lambda_b \to \Lambda_c$ semileptonic decay.

III. $\bar{B} \to D$ AND $\bar{B} \to D^*$ SEMILEPTONIC DECAY RESULTS WITH AN UNPOLARIZED FINAL τ LEPTON

We present now results for the $\bar{B} \to D\tau\bar{\nu}_\tau$ and $\bar{B} \to D^*\tau\bar{\nu}_\tau$ semileptonic decays. As in the previous section, we

TABLE II. $\mathcal{R}_D$ and $\mathcal{R}_{D^*}$ ratios obtained in the SM and with NP effects from Ref. [31].

	SM	Fit 6	Fit 7
$\mathcal{R}_D = \frac{\Gamma(\bar{B}\to D\tau\bar{\nu}_\tau)}{\Gamma(\bar{B}\to D\ell\bar{\nu}_\ell)}$	0.300 ± 0.005	0.405 ± 0.048	0.389 ± 0.045
$\mathcal{R}_{D^*} = \frac{\Gamma(\bar{B}\to D^*\tau\bar{\nu}_\tau)}{\Gamma(\bar{B}\to D^*\ell\bar{\nu}_\ell)}$	0.251 ± 0.004	0.302 ± 0.014	0.306 ± 0.013

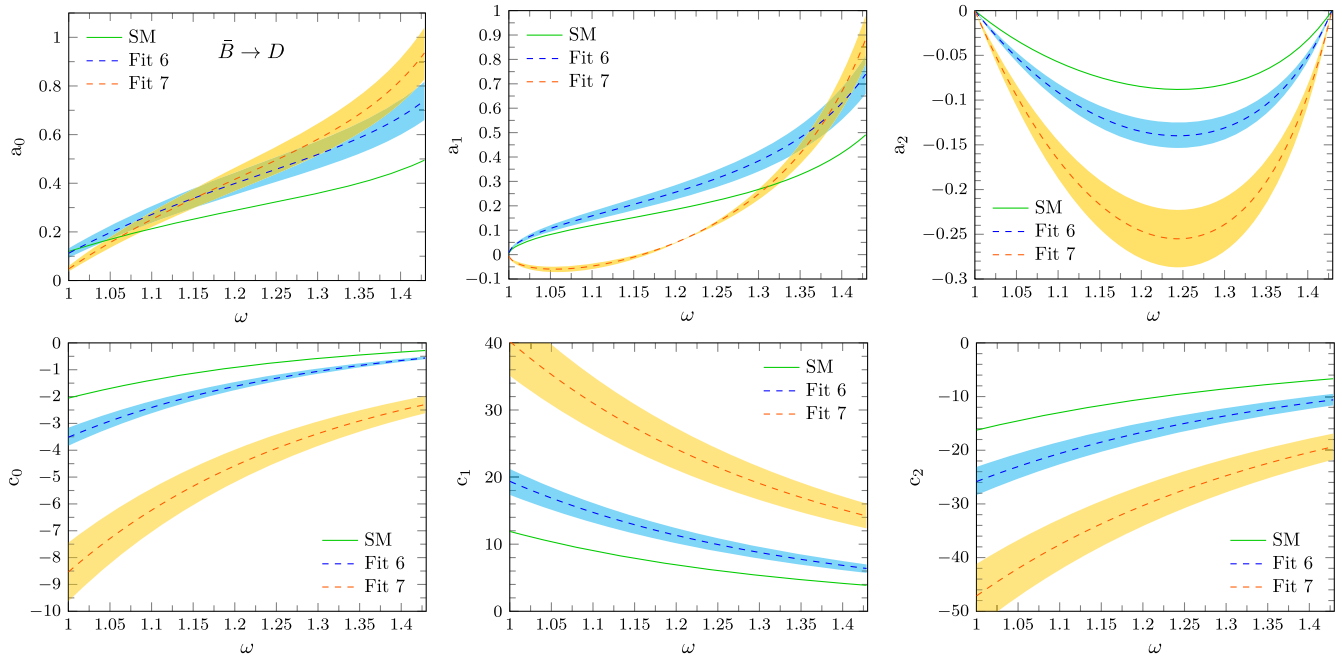

FIG. 17. $\bar{B} \to D\tau\bar{\nu}_\tau$ decay: $a_{0,1,2}$ c.m. angular and $c_{0,1,2}$ LAB energy expansion coefficients as a function of ω. Uncertainty bands are as in Fig. 16.

shall use the Wilson coefficients and form factors corresponding to fits 6 and 7 in Ref. [31]. The form factors are taken from Ref. [15], but in Ref. [31] not only the Wilson coefficients but also the $1/m_{b,c}$ and $1/m_c^2$ corrections to the form factors are simultaneously fitted to experimental data. To estimate the theoretical uncertainties, for each fit, we shall use different sets of Wilson coefficients and form factors, selected such that the χ^2 merit function computed in [31] changes at most by one unit from its value at the fit minimum. With those sets, for each of the observables that we calculate we determine the maximum deviations above and below their central values. These deviations will give us the 1σ theoretical uncertainty and it will be shown as an error band in the figures below.

We start by showing in Fig. 16 the $d\Gamma/d\omega$ differential decay width. Both NP fits give similar results that differ from the SM distribution. The corresponding predictions for the $\mathcal{R}_D$ and $\mathcal{R}_{D^*}$ ratios are given in Table II. The ratios obtained with NP are in agreement with present experimental results, though they are located at the high-value corner of the allowed regions, since they were fitted in Ref. [31] to the previous HFLAV world average values quoted in [2].[8] Again, we notice that for these quantities both fits are equivalent within errors and other observables are needed in order to decide between different NP explanations of the experimental data.

These observables can be the $a_{0,1,2}$ and $c_{0,1,2}$ coefficients in the c.m. angular $d^2\Gamma/(d\omega d\cos\theta_\ell)$ and LAB energy $d^2\Gamma/(d\omega dE_\ell)$ distributions. They are shown in Figs. 17 and 18 for the $\bar{B} \to D\tau\bar{\nu}_\tau$ and $\bar{B} \to D^*\tau\bar{\nu}_\tau$ decays, respectively. With the only exception of a_0, all of them can be used to distinguish between the two fits. However, for the $\bar{B} \to D^*$, and similar to what happened for the $\bar{B}_c \to J/\psi$ decay, SM results for some of these coefficients fall within the error band of those obtained from NP fit 6. In fact the ω-shape patterns exhibited in Figs. 17 and 18 for the $\bar{B} \to D^{(*)}$ reactions are qualitatively similar to those found in Sec. II for the $\bar{B}_c$ decays.

We stress that the LAB $d^2\Gamma(\bar{B} \to D^{(*)}\tau\bar{\nu}_\tau)/(d\omega dE_\ell)$ differential decay widths are reported for the very first time in this work. Though, as shown in [33], c.m. and LAB unpolarized distributions provide access to equivalent dynamical information [invariant functions $\mathcal{A}(\omega)$, $\mathcal{B}(\omega)$ and $\mathcal{C}(\omega)$ defined in Eq. (14) of that reference], it should be explored if the LAB observables could be measured with better precision.

In Fig. 19 we show the c.m. forward-backward asymmetry [Eq. (8)]. The shape in each case is very similar to what we obtained respectively for $\bar{B}_c \to \eta_c$ and $\bar{B}_c \to J/\psi$ decays, see Fig. 8, with very close values at maximum recoil and significantly smaller errors.

To minimize experimental and theoretical uncertainties, it was proposed in Ref. [33] to pay attention to the ratio $\mathcal{R}(\mathcal{A}_{\rm FB})$, defined as

$$\mathcal{R}(\mathcal{A}_{\rm FB}) = \frac{(\mathcal{A}_{\rm FB})_\tau}{(\mathcal{A}_{\rm FB})^{\rm SM}_{\ell=e,\mu}} = \frac{\left[\frac{a_1}{2a_0+2a_2/3}\right]_\tau}{\left[\frac{a_1}{2a_0+2a_2/3}\right]^{\rm SM}_{\ell=e,\mu}}. \quad (15)$$

In Fig. 20, we show the theoretical predictions for $\mathcal{R}(\mathcal{A}_{\rm FB})$ for the $\bar{B}_c \to J/\psi$, $\bar{B} \to D^*$ and $\Lambda_b \to \Lambda_c$ semileptonic

[8]In the latest HFLAV average [1], a measurement by the *BABAR* collaboration [79] is omitted, because it does not allow for a separation of the different isospin modes.

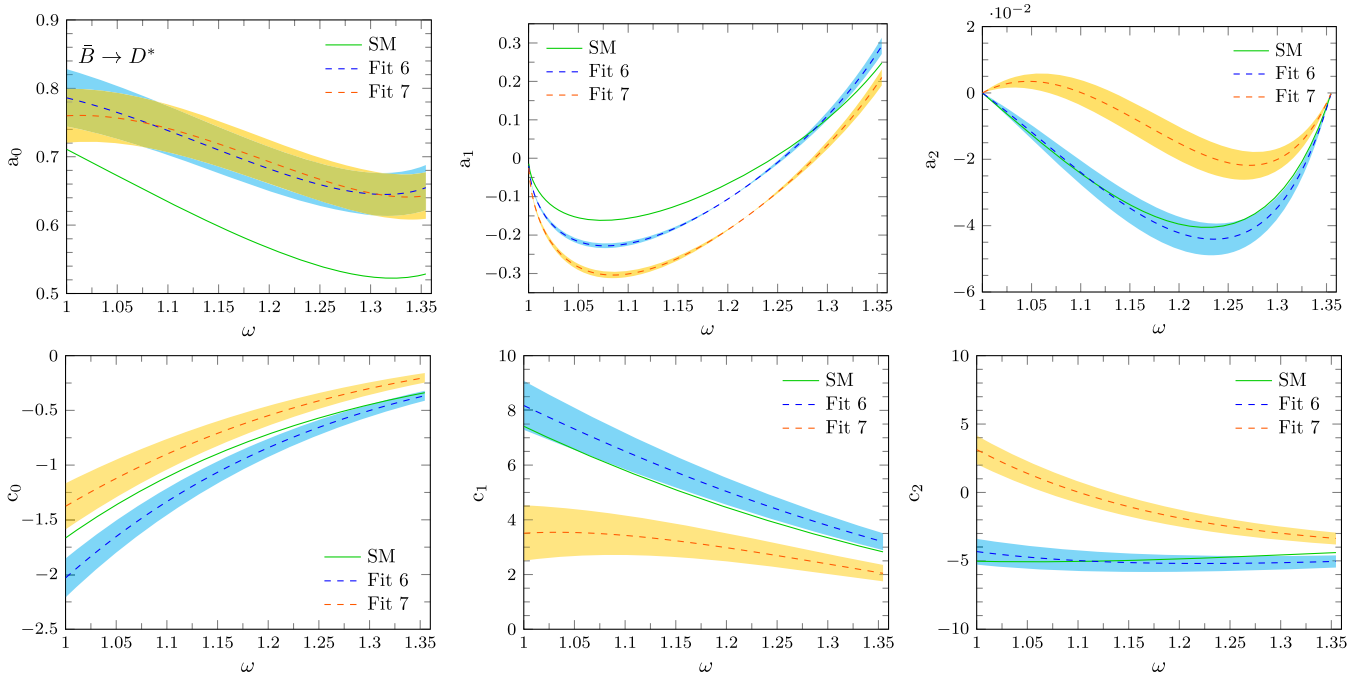

FIG. 18. $\bar{B} \to D^* \tau \bar{\nu}_\tau$ decay: $a_{0,1,2}$ c.m. angular and $c_{0,1,2}$ LAB energy expansion coefficients as a function of ω. Uncertainty bands are as in Fig. 16.

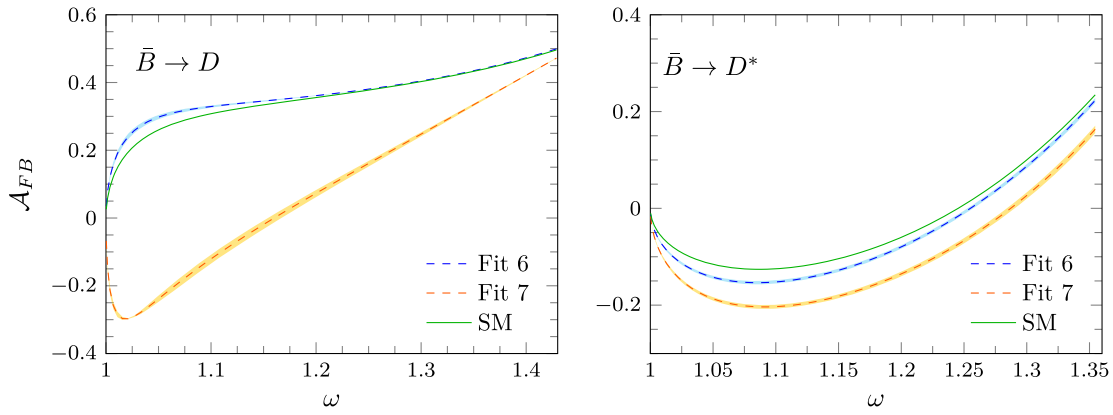

FIG. 19. Forward-backward asymmetry in the c.m. reference frame for the $\bar{B} \to D \tau \bar{\nu}_\tau$ (left) and $\bar{B} \to D^* \tau \bar{\nu}_\tau$ (right) decays. Uncertainty bands are as in Fig. 16.

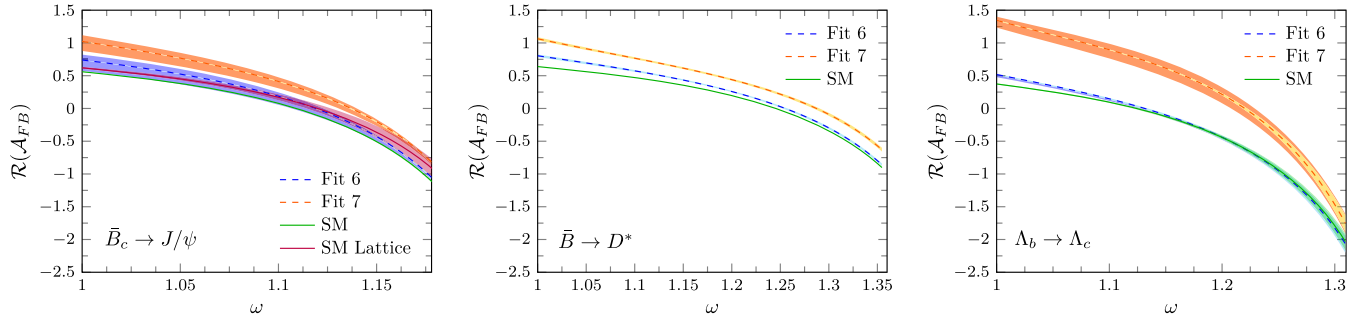

FIG. 20. $\mathcal{R}(\mathcal{A}_{\rm FB})$ ratios defined in Eq. (15) for the $\bar{B}_c \to J/\psi$, $\bar{B} \to D^*$ and $\Lambda_b \to \Lambda_c$ semileptonic decays, as a function of ω. Errors bands have been calculated as in Figs. 2 and 16 for the $\bar{B}_c$ and $\bar{B}$ meson decays. The Λ_b plot has been taken from Fig. 4 of Ref. [33], while for the $\bar{B}_c \to J/\psi$ decay, we also show the SM results obtained with LQCD form factors from Ref. [62].

decays, with the latter taken from Ref. [33] where details of the LQCD form factors used in the calculation can be found. In addition, for $\bar{B}_c \to J/\psi$, we also display the SM results obtained with LQCD form factors from Ref. [62], which agree remarkably well with the NRQM distribution. Note that for $\bar{B}_c \to \eta_c$ and $\bar{B} \to D$ decays, the denominator in Eq. (15) vanishes in the massless lepton limit ($m_\ell \to 0$), since $a_1(\omega) = a_1(\omega, h = -1) + a_1(\omega, h = +1)$, and the negative helicity contribution is zero [Eq. (11)], while the positive helicity one is proportional to m_ℓ.

The ratio $\mathcal{R}(\mathcal{A}_{\rm FB})$ can be measured by subtracting the number of events seen for $\theta_\ell \in [0, \pi/2]$ and for $\theta_\ell \in [\pi/2, \pi]$ and dividing by the total sum of observed events, in each of the $H_b \to H_c \tau \bar{\nu}_\tau$ and $H_b \to H_c e(\mu) \bar{\nu}_{e(\mu)}$ reactions. We expect that this observable should be free of a good part of experimental normalization errors. On the theoretical side, we see in Fig. 20 that predictions for this ratio have indeed small uncertainties, and that this quantity has the potential to establish the validity of the NP scenarios associated to fit 7, even more if all three reactions shown in Fig. 20 are simultaneously confronted with experiment.

For completeness, $\bar{B} \to D^{(*)}$ results with a polarized final τ are given in Appendix D. Roughly, the same qualitative features that we have discussed for the polarized $\bar{B}_c \to \eta_c$ and $\bar{B}_c \to J/\psi$ semileptonic decays are also found in this case.

IV. CONCLUSIONS

We have shown the relevant role that the $a_{0,1,2}(\omega)$ c.m. and $c_{0,1,2}(\omega)$ LAB scalar functions, in terms of which the c.m. $d^2\Gamma/(d\omega d\cos\theta_\ell)$ and LAB $d^2\Gamma/(d\omega dE_\ell)$ differential decay widths are expanded, could play in order to separate between different NP scenarios that otherwise give rise to the same $\mathcal{R}_{D^{(*)}}, \mathcal{R}_{\eta_c, J/\psi}$ ratios. The scheme we have used is the one originally developed in Ref. [33], and applied there to the analysis of the $\Lambda_b \to \Lambda_c \tau \bar{\nu}_\tau$ decay, which we have extended in this work to the study of the $\bar{B} \to D, \bar{B} \to D^*, \bar{B}_c \to \eta_c$ and $\bar{B}_c \to J/\psi$ meson reactions.

For the $\bar{B}_c \to \eta_c, J/\psi$ transitions we have obtained results from a NRQM scheme, consistent with the expected breaking pattern of HQSS from $\bar{B} \to D^{(*)}$ decays [80], estimating the systematic uncertainties caused by the use of different interquark potentials. Besides, and since SM LQCD vector and axial form factors for $\bar{B}_c \to J/\psi$ have recently been reported by the HPQCD collaboration [62], we have made systematic comparisons with the SM observables computed with the LQCD input. In general, though there appear some overall normalization inconsistencies, we find quite good agreements for ω shapes, which become much better for observables constructed out of ratios of distributions, like the τ-forward-backward [$\mathcal{A}_{\rm FB}$] and τ-polarization [$\mathcal{A}_{\lambda_\tau}$] asymmetries, as well as the ratios between predictions obtained in τ and (e/μ) modes like $\mathcal{R}_{J/\psi}$ (Table I) or $\mathcal{R}(\mathcal{A}_{\rm FB})$ (Fig. 20). This further supports the reliability of our results for the LAB or the $\bar{B} \to \eta_c$ distributions, not yet studied.

As a general rule, the $\bar{B}_c \to J/\psi$ observables, even involving τ polarization, are less optimal for distinguishing between NP scenarios than those obtained from $\bar{B}_c \to \eta_c$ decays, or those discussed in Ref. [33] for the related $\Lambda_b \to \Lambda_c$ semileptonic decay. We have also found qualitative similar behaviors for $\bar{B} \to D$ and $\bar{B}_c \to \eta_c$, and $\bar{B} \to D^*$ and $\bar{B}_c \to J/\psi$ decay observables.

We have also drawn attention to the ratio $\mathcal{R}(\mathcal{A}_{\rm FB})$, defined in Eq. (15) and shown in Fig. 20 for $\bar{B}_c \to J/\psi$, $\bar{B} \to D^*$ and $\Lambda_b \to \Lambda_c$ decays, as a promising quantity, both from the experimental and theoretical points of view, to shed light into details of different NP scenarios in $b \to c \tau \bar{\nu}_\tau$ transitions.

One should notice however that the effective Hamiltonian of Eq. (3), despite excluding right-handed neutrino terms, contains five, complex in general, NP Wilson coefficients. While one of them can always be taken to be real, that still leaves nine free parameters to be determined from data. Even assuming that the form factors were known, and therefore the genuinely hadronic part (W) of the $\tilde{W}$ SFs, it would be difficult to determine all NP parameters just from the study of a unique reaction. As shown in Ref. [33], for decays with an unpolarized final τ lepton, the c.m. $d^2\Gamma/(d\omega d\cos\theta_\ell)$ and LAB $d^2\Gamma/(d\omega dE_\ell)$ differential decay widths are completely determined by only three independent functions which are linear combinations of the $\tilde{W}$ SFs, the latter depending on the NP Wilson coefficients. This means that $a_{0,1,2}(\omega)$ and $c_{0,1,2}(\omega)$ contain the same information. For the case of polarized final τ's, the c.m. $d^2\Gamma/(d\omega d\cos\theta_\ell)$ and LAB $d^2\Gamma/(d\omega dE_\ell)$ distributions provide complementary information giving access to another five independent linear combinations of the $\tilde{W}$'s [33]. But in this case it is the experimental measurement of the required polarized decay that could become a very difficult task. We think it is therefore more convenient to analyze data from various types of semileptonic decays simultaneously (e.g., $\bar{B} \to D, \bar{B} \to D^*, \Lambda_b \to \Lambda_c, \bar{B}_c \to \eta_c$, $\bar{B}_c \to J/\psi \ldots$), considering both the e/μ and τ modes. The scheme presented in [33] is a powerful tool to achieve this objective.

ACKNOWLEDGMENTS

We warmly thank C. Murgui, A. Peñuelas and A. Pich for useful discussions. This research has been supported by the Spanish Ministerio de Economía y Competitividad (MINECO) and the European Regional Development Fund (ERDF) under Contracts No. FIS2017-84038-C2-1-P, No. FPA2016-77177-C2-2-P and No. PID2019-105439G-C22, by Generalitat Valenciana under Contract No. PROMETEO/2020/023 and by the EU STRONG-2020 project under the program H2020-INFRAIA-2018-1, Grant Agreement No. 824093.

APPENDIX A: FORM FACTORS FOR $P_b(0^-) \to P_c(0^-)$ AND $P_b(0^-) \to P_c^*(1^-)$ TRANSITIONS

For these two transitions we use the standard definitions of the form factors taken from Ref. [15],[9]

(i) $P_b \to P_c$

$$\begin{aligned}
\langle P_c;\vec{p}\,'|\bar{c}(0)b(0)|P_b;\vec{p}\rangle &= \frac{1+\omega}{2}h_S(\omega)\\
\langle P_c;\vec{p}\,'|\bar{c}(0)\gamma_5 b(0)|P_b;\vec{p}\rangle &= \langle P_c;\vec{p}\,'|\bar{c}(0)\gamma^\alpha\gamma_5 b(0)|P_b;\vec{p}\rangle = 0\\
\langle P_c;\vec{p}\,'|\bar{c}(0)\gamma^\alpha b(0)|P_b;\vec{p}\rangle &= \frac{1}{2}(v^\alpha + v'^\alpha)h_+(\omega) + \frac{1}{2}(v^\alpha - v'^\alpha)h_-(\omega)\\
\langle P_c;\vec{p}\,'|\bar{c}(0)\sigma^{\alpha\beta} b(0)|P_b;\vec{p}\rangle &= \frac{i}{2}(v'^\alpha v^\beta - v'^\beta v^\alpha)h_T(\omega)\\
\langle P_c;\vec{p}\,'|\bar{c}(0)\sigma^{\alpha\beta}\gamma_5 b(0)|P_b;\vec{p}\rangle &= \frac{1}{2}\epsilon^{\alpha\beta\delta\eta}v'_\delta v_\eta h_T(\omega)
\end{aligned} \tag{A1}$$

with $v^\alpha = p^\alpha/M$ and $v'^\alpha = p'^\alpha/M' = (p^\alpha - q^\alpha)/M'$, the quadrivelocities of the initial and final hadrons, which have masses M and M', respectively, $\omega = (v\cdot v')$ and $\epsilon_{0123} = +1$.

(ii) $P_b \to P_c^*$

$$\begin{aligned}
\langle P_c^*;\vec{p}\,',r|\bar{c}(0)b(0)|P_b;\vec{p}\rangle &= 0\\
\langle P_c^*;\vec{p}\,',r|\bar{c}(0)\gamma_5 b(0)|P_b;\vec{p}\rangle &= -\frac{1}{2}(\epsilon_r^*\cdot v)h_P(\omega)\\
\langle P_c^*;\vec{p}\,',r|\bar{c}(0)\gamma^\alpha b(0)|P_b;\vec{p}\rangle &= \frac{i}{2}\epsilon^\alpha{}_{\delta\eta\gamma}\epsilon_r^{*\delta}v'^\eta v^\gamma h_V(\omega)\\
\langle P_c^*;\vec{p}\,',r|\bar{c}(0)\gamma^\alpha\gamma_5 b(0)|P_b;\vec{p}\rangle &= \frac{\omega+1}{2}\epsilon_r^{*\alpha}h_{A_1}(\omega) - \frac{(\epsilon_r^*\cdot v)}{2}[v^\alpha h_{A_2}(\omega) + v'^\alpha h_{A_3}(\omega)]\\
\langle P_c^*;\vec{p}\,',r|\bar{c}(0)\sigma^{\alpha\beta} b(0)|P_b;\vec{p}\rangle &= -\frac{1}{2}\epsilon^{\alpha\beta}{}_{\delta\eta}\{\epsilon_r^{*\delta}[(v^\eta + v'^\eta)h_{T_1}(\omega) + (v^\eta - v'^\eta)h_{T_2}(\omega)] + v^\delta v'^\eta(\epsilon_r^*\cdot v)h_{T_3}(\omega)\}\\
\langle P_c^*;\vec{p}\,',r|\bar{c}(0)\sigma^{\alpha\beta}\gamma_5 b(0)|P_b;\vec{p}\rangle &= -\frac{i}{2}\{\epsilon_r^{*\alpha}[(v^\beta + v'^\beta)h_{T_1}(\omega) + (v^\beta - v'^\beta)h_{T_2}(\omega)]\\
&\quad - \epsilon_r^{*\beta}[(v^\alpha + v'^\alpha)h_{T_1}(\omega) + (v^\alpha - v'^\alpha)h_{T_2}(\omega)] + (v^\alpha v'^\beta - v^\beta v'^\alpha)(\epsilon_r^*\cdot v)h_{T_3}(\omega)\},
\end{aligned} \tag{A2}$$

where r is the helicity of the final vector meson, with ϵ_r its corresponding polarization vector. In short,

$$\langle P_c^*;\vec{p}\,',r|\bar{c}(0)\Gamma^{(\alpha\beta)}b(0)|P_b;\vec{p}\rangle = T_\mu^{(\alpha\beta)}\epsilon_r^{\mu *} \tag{A3}$$

with $\Gamma^{(\alpha\beta)} = 1,\gamma_5,\gamma^\alpha,\gamma^\alpha\gamma_5,\sigma^{\alpha\beta}$ and $\sigma^{\alpha\beta}\gamma_5$ and $T_\mu^{(\alpha\beta)}$ read from Eq. (A2).

The form factors are real functions of ω greatly constrained by HQSS near zero recoil ($\omega = 1$) [15,80]. Indeed, all factors in Eqs. (A1) and (A2) have been chosen such that in the heavy quark limit each form factor either vanishes or equals the leading-order Isgur-Wise function[10]

[9]Note however that within the conventions of Ref. [33], which we follow here, our hadronic matrix elements are dimensionless and they should be compared to those given in [15] divided by a $\sqrt{2M}\sqrt{2M'}$ factor.

[10]These relations trivially follow from

$$\langle P_c^{(*)};\vec{p}\,',(r)|\bar{c}(0)\Gamma b(0)|P_b;\vec{p}\rangle = -\frac{1}{2}\xi(\omega)\mathrm{Tr}[\bar{H}_{v'}^{(c)}\Gamma H_v^{(b)}], \tag{A4}$$

where the pseudoscalar and vector mesons are represented by a superfield, which has the right transformation properties under heavy quark and Lorentz symmetry [15,80]

$$H_v^{(Q)} = \frac{1+\not{v}}{2}(V_v^{(Q)}\not{\epsilon} - P_v^{(Q)}\gamma_5) \tag{A5}$$

and $\bar{H}_v^{(Q)} = \gamma^0 H_v^{(Q)\dagger}\gamma^0$. For $\bar{B}_c \to \eta_c, J/\psi$ transitions, the appropriate 4×4 field accounts also for the heavy anticharm quark both in the initial and final mesons [81]

$$H_v^{(Q\bar{c})} = \frac{1+\not{v}}{2}(V_v^{(Q\bar{c})}\not{\epsilon} - P_v^{(Q\bar{c})}\gamma_5)\frac{1-\not{v}}{2}. \tag{A6}$$

$$h_- = h_{A_2} = h_{T_2} = h_{T_3} = 0,$$
$$h_+ = h_V = h_{A_1} = h_{A_3} = h_S = h_P = h_T = h_{T_1} = \xi. \quad \text{(A7)}$$

The hadron tensors and $\tilde{W}$ SFs introduced in Ref. [33] are straightforwardly obtained from Eq. (A1) in the case of $P_b \to P_c$ transitions, while for decays into vector mesons, we use

$$\sum_r \langle P_c^*; \vec{p}', r|\bar{c}(0)\Gamma^{(\alpha\beta)}b(0)|P_b; \vec{p}\rangle \times \langle P_c^*; \vec{p}', r|\bar{c}(0)\Gamma^{(\rho\lambda)}b(0)|P_b; \vec{p}\rangle^* = T_\mu^{(\alpha\beta)}T_\nu^{(\rho\lambda)}(-g^{\mu\nu} + v'^\mu v'^\nu). \quad \text{(A8)}$$

The explicit expressions for the $\tilde{W}$ SFs in terms of the above form factors and the Wilson coefficients are given in the following Appendix.

APPENDIX B: HADRON TENSOR $\tilde{W}$ SFs FOR THE $P_b \to P_c \ell^- \bar{\nu}_\ell$ AND $P_b \to P_c^* \ell^- \bar{\nu}_\ell$ DECAYS

We compile here the $\tilde{W}$ SFs introduced in Ref. [33] for the particular meson decays studied in this work. As shown in that reference, these $\tilde{W}$ SFs determine the LAB $d^2\Gamma/(d\omega dE_\ell)$ and c.m. $d^2\Gamma/(d\omega d\cos\theta_\ell)$ differential decay widths, for the full set of NP operators in Eq. (3), for generally complex Wilson coefficients, and for the case where the final charged lepton has a well-defined helicity in either reference frame. In the equations below, we use $C_{V,A} = (1 + C_{V_L} \pm C_{V_R})$ and $C_{S,P} = (C_{S_L} \pm C_{S_R})$.

1. $P_b \to P_c \ell^- \bar{\nu}_\ell$

In this case, the SFs related to the SM currents are

$$\tilde{W}_1 = \tilde{W}_3 = 0, \qquad \tilde{W}_2 = \frac{|C_V|^2}{r}F_+^2,$$
$$\tilde{W}_4 = \frac{|C_V|^2}{4r}(F_+ - F_-)^2, \qquad \tilde{W}_5 = \frac{|C_V|^2}{r}F_+(F_- - F_+), \quad \text{(B1)}$$

where

$$F_+ = \frac{1}{R}\left(h_+ - \frac{1-r}{1+r}h_-\right), \qquad F_- = \frac{1}{R}\left(h_- - \frac{1-r}{1+r}h_+\right) = \frac{1-r^2}{1+r^2-2r\omega}(F_0 - F_+)$$
$$F_0 = \frac{2r(1+\omega)}{R(1+r)^2}\left[h_+ - \frac{1+r}{1-r}\frac{\omega-1}{\omega+1}h_-\right] \quad \text{(B2)}$$

with $r = M'/M$ and $R = 2\sqrt{r}/(1+r)$, and we have also introduced the F_0 form factor in the definition of F_-, as commonly done in this type of calculations. In addition,

$$\tilde{W}_{SP} = |C_S|^2\left(\frac{1+\omega}{2}\right)^2 h_S^2, \qquad \tilde{W}_{I1} = C_V C_S^* \frac{1+\omega}{\sqrt{r}}h_S F_+, \qquad \tilde{W}_{I2} = C_V C_S^* \frac{1+\omega}{2\sqrt{r}}h_S(F_- - F_+),$$
$$\tilde{W}_{I3} = -C_T^* C_S \frac{1+\omega}{2r}h_S h_T, \qquad \tilde{W}_{I4} = -C_T^* C_V \frac{h_T F_+}{r^{3/2}}, \qquad \tilde{W}_{I5} = C_T^* C_V \frac{h_T(F_+ - F-)}{2r^{3/2}}, \qquad \tilde{W}_{I6} = \tilde{W}_{I7} = 0,$$
$$\tilde{W}_1^T = \frac{|C_T|^2}{4}(\omega^2 - 1)h_T^2, \qquad \tilde{W}_2^T = \frac{|C_T|^2}{4r^2}(1 + r^2 - 2r\omega)h_T^2, \qquad \tilde{W}_3^T = \frac{|C_T|^2}{4r^2}h_T^2,$$
$$\tilde{W}_4^T = -\frac{|C_T|^2}{4r^2}(1 - r\omega)h_T^2, \qquad \tilde{W}_5^T = 0. \quad \text{(B3)}$$

As derived in Ref. [33], the tensor $\tilde{W}$ SFs accomplish

$$2\tilde{W}_1^T + \tilde{W}_2^T + (1 - 2r\omega + r^2)\tilde{W}_3^T + 2(1 - r\omega)\tilde{W}_4^T = 0. \quad \text{(B4)}$$

2. $P_b \to P_c^* \ell^- \bar{\nu}_\ell$

In this case, the $\tilde{W}$ SFs related to the SM currents are

$$\begin{aligned}
\tilde{W}_1 &= \frac{|C_V|^2}{4}(\omega^2-1)h_V^2 + \frac{|C_A|^2}{4}(\omega+1)^2 h_{A_1}^2 \\
\tilde{W}_2 &= -\frac{|C_V|^2}{4r^2}(1+r^2-2r\omega)h_V^2 + \frac{|C_A|^2}{4r^2}(\omega+1)^2\left(h_{A_1}^2 - 2\frac{\omega-r}{\omega+1}h_{A_1}(rh_{A_2}+h_{A_3}) + \frac{\omega-1}{\omega+1}(rh_{A_2}+h_{A_3})^2\right) \\
\tilde{W}_3 &= \frac{\mathrm{Re}[C_V C_A^*]}{r}(\omega+1)h_V h_{A_1} \\
\tilde{W}_4 &= -\frac{|C_V|^2}{4r^2}h_V^2 + \frac{|C_A|^2}{4r^2}(\omega+1)^2(h_{A_1}-h_{A_3})\left(h_{A_1} + \frac{1-\omega}{1+\omega}h_{A_3}\right) \\
\tilde{W}_5 &= \frac{|C_V|^2}{2r^2}(1-r\omega)h_V^2 - \frac{|C_A|^2}{2r^2}\{(1+\omega)(h_{A_1}-rh_{A_2}-h_{A_3})[(1+\omega)h_{A_1}-(\omega-r)h_{A_3}] \\
&\quad + (1+\omega)(rh_{A_2}+h_{A_3})(h_{A_1}-(1-r)h_{A_3})\}.
\end{aligned} \tag{B5}$$

The rest of NP $\tilde{W}$ SFs are

$$\begin{aligned}
\tilde{W}_{SP} &= \frac{|C_P|^2}{4}(\omega^2-1)h_P^2 \\
\tilde{W}_{I1} &= \frac{C_A C_P^*}{2r}(\omega^2-1)\left[rh_{A_2}+h_{A_3} - \frac{\omega-r}{\omega-1}h_{A_1}\right]h_P \\
\tilde{W}_{I2} &= \frac{C_A C_P^*}{2r}(\omega+1)[\omega h_{A_1} + (1-\omega)h_{A_3}]h_P \\
\tilde{W}_{I3} &= -\frac{C_P C_T^*}{2r}(\omega^2-1)h_P T_1 \\
\tilde{W}_{I4} &= \frac{C_V C_T^*}{2r^2}[(1-r\omega)T_2 + (\omega-r)T_3]h_V - \frac{C_A C_T^*}{2r^2}\{(\omega+1)h_{A_1}[(r-\omega)T_1 + rT_2 + T_3] + (\omega^2-1)(rh_{A_2}+h_{A_3})T_1\} \\
\tilde{W}_{I5} &= -\frac{C_V C_T^*}{2r^2}(T_2+\omega T_3)h_V + \frac{C_A C_T^*}{2r^2}\{(\omega^2-1)h_{A_3}T_1 - (\omega+1)h_{A_1}[\omega T_1 - T_3]\} \\
\tilde{W}_{I6} &= \frac{C_V C_T^*}{2r}(\omega^2-1)h_V(rT_2+T_3) - \frac{C_A C_T^*}{2r}(\omega+1)h_{A_1}[(1-r\omega)T_2 + (\omega-r)T_3] \\
\tilde{W}_{I7} &= -\frac{C_V C_T^*}{2r}(\omega^2-1)h_V T_3 + \frac{C_A C_T^*}{2r}(\omega+1)h_{A_1}[T_2+\omega T_3] \\
\tilde{W}_1^T &= \frac{|C_T|^2}{4}(\omega^2-1)^2 T_1^2 \\
\tilde{W}_2^T &= \frac{|C_T|^2}{4r^2}[(r^2-2r\omega+1)(\omega^2-1)T_1^2 + (1-r^2)(T_3^2-T_2^2) + 2r(1-r\omega)(\omega T_2+T_3)T_2 + 2(r-\omega)(T_2+\omega T_3)T_3] \\
\tilde{W}_3^T &= \frac{|C_T|^2}{4r^2}[(\omega^2-1)(T_1^2-T_3^2) - (T_2+\omega T_3)^2] \\
W_4^T &= \frac{|C_T|^2}{4r^2}[(1-r\omega)(T_2^2+T_3^2) + 2(\omega-r)T_2T_3 + (\omega^2-1)(2T_3^2-(1-r\omega)T_1^2)] \\
\tilde{W}_5^T &= 0
\end{aligned} \tag{B6}$$

with the tensor $\tilde{W}^T_{1,2,3,4}$ SFs satisfying Eq. (B4), and

$$T_1 = \frac{(\omega+1)h_{T_1} + (\omega-1)h_{T_2}}{\omega^2-1} - h_{T_3},$$
$$T_2 = -\frac{(\omega+1)h_{T_1} + (\omega-1)h_{T_2}}{\omega^2-1},$$
$$T_3 = \frac{(\omega+1)h_{T_1} - (\omega-1)h_{T_2}}{\omega^2-1}. \tag{B7}$$

Although T_1, T_2 and T_3 behave as $\pm 1/(\omega-1)$ in the heavy quark limit, the corresponding $\tilde{W}^T_{1,2,3,4}$ SFs are finite at zero recoil, as they should be, with their values being given by $|C_T|^2[1, -\frac{r^2+6r+1}{4r^2}, -\frac{1}{4r^2}, \frac{3r+1}{4r^2}]$, respectively.

APPENDIX C: EVALUATION OF THE $\bar{B}_c \to \eta_c$ AND $\bar{B}_c \to J/\psi$ SEMILEPTONIC DECAY FORM FACTORS WITHIN THE NRQM OF REF. [19]

Within the NRQM calculation of Ref. [19], and with the global phases used in the present work, we obtain the following expressions for the different form factors.

1. $\bar{B}_c \to \eta_c$

For the pseudoscalar-pseudoscalar $\bar{B}_c \to \eta_c$ transition we have

$$F_+ = \frac{1}{2M}\left(V^0 + V^3\frac{E'-M}{|\vec{q}|}\right), \quad F_- = \frac{1}{2M}\left(V^0 + V^3\frac{E'+M}{|\vec{q}|}\right), \quad h_S = \frac{S}{(\omega+1)\sqrt{MM'}}, \quad h_T = -\sqrt{\frac{M'}{M}}i\frac{T^{03}}{|\vec{q}|}, \tag{C1}$$

with $F_\pm$ defined in Eq. (B2), and where V^μ, S and $T^{\mu\nu}$ stand for the NRQM matrix elements of the vector, scalar and tensor $b \to c$ transition currents, respectively. In addition, $E' = \sqrt{M'^2 + \vec{q}^2}$ is the energy of the final meson that has three-momentum $-\vec{q}$ in the LAB frame, with $\vec{q}$ the three-momentum transferred in the LAB frame and that for the purpose of calculation we take it along the positive Z axis. For the matrix elements one has the results:

$$V^0 = \sqrt{2M2E'}\int d^3p \frac{1}{4\pi}[\hat{\phi}^{(\eta_c)}(|\vec{p}|)]^*\hat{\phi}^{(\bar{B}_c)}\left(\left|\vec{p}-\frac{1}{2}\vec{q}\right|\right)\sqrt{\frac{\hat{E}_c\hat{E}_b}{4E_cE_b}}\left(1+\frac{(-\frac{1}{2}\vec{q}-\vec{p})\cdot(\frac{1}{2}\vec{q}-\vec{p})}{\hat{E}_c\hat{E}_b}\right),$$
$$V^3 = \sqrt{2M2E'}\int d^3p \frac{1}{4\pi}[\hat{\phi}^{(\eta_c)}(|\vec{p}|)]^*\hat{\phi}^{(\bar{B}_c)}\left(\left|\vec{p}-\frac{1}{2}\vec{q}\right|\right)\sqrt{\frac{\hat{E}_c\hat{E}_b}{4E_cE_b}}\left(\frac{\frac{1}{2}|\vec{q}|-p_z}{\hat{E}_b}+\frac{-\frac{1}{2}|\vec{q}|-p_z}{\hat{E}_c}\right),$$
$$S = \sqrt{2M2E'}\int d^3p \frac{1}{4\pi}[\hat{\phi}^{(\eta_c)}(|\vec{p}|)]^*\hat{\phi}^{(\bar{B}_c)}\left(\left|\vec{p}-\frac{1}{2}\vec{q}\right|\right)\sqrt{\frac{\hat{E}_c\hat{E}_b}{4E_cE_b}}\left(1-\frac{(-\frac{1}{2}\vec{q}-\vec{p})\cdot(\frac{1}{2}\vec{q}-\vec{p})}{\hat{E}_c\hat{E}_b}\right),$$
$$T^{03} = i\sqrt{2M2E'}\int d^3p \frac{1}{4\pi}[\hat{\phi}^{(\eta_c)}(|\vec{p}|)]^*\hat{\phi}^{(\bar{B}_c)}\left(\left|\vec{p}-\frac{1}{2}\vec{q}\right|\right)\sqrt{\frac{\hat{E}_c\hat{E}_b}{4E_cE_b}}\left(\frac{\frac{1}{2}|\vec{q}|-p_z}{\hat{E}_b}-\frac{-\frac{1}{2}|\vec{q}|-p_z}{\hat{E}_c}\right). \tag{C2}$$

Here, $\hat{\phi}$ stands for the orbital part of the meson wave functions in momentum space and $\hat{E}_f = E_f + m_f$, with m_f, E_f the mass and relativistic energy of the quark with flavor f. The corresponding three-momenta are $\frac{1}{2}\vec{q}-\vec{p}$ for the quark b and $-\frac{1}{2}\vec{q}-\vec{p}$ for the quark c.

2. $\bar{B}_c \to J/\psi$

For the pseudoscalar-vector $\bar{B}_c \to J/\psi$ transition we now have

$$h_V = \frac{M'\sqrt{2}}{|\vec{q}|}\frac{V^1_{\lambda=-1}}{\sqrt{MM'}}, \quad h_P = \frac{M'}{|\vec{q}|}\frac{P_{\lambda=0}}{\sqrt{MM'}},$$
$$h_{A_1} = \frac{\sqrt{2}}{\omega+1}\frac{A^1_{\lambda=-1}}{\sqrt{MM'}}, \quad h_{A_2} = -\frac{M'}{|\vec{q}|}\left[-\frac{A^0_{\lambda=0}}{\sqrt{MM'}} - \frac{E'}{|\vec{q}|}\frac{A^3_{\lambda=0}}{\sqrt{MM'}} + \sqrt{2}\frac{M'}{|\vec{q}|}\frac{A^1_{\lambda=-1}}{\sqrt{MM'}}\right], \quad h_{A_3} = -\frac{M'^2}{|\vec{q}|^2}\left(\frac{A^3_{\lambda=0}}{\sqrt{MM'}} - \sqrt{2}\frac{E'}{M'}\frac{A^1_{\lambda=-1}}{\sqrt{MM'}}\right),$$
$$T_1 = \frac{M'^2}{|\vec{q}|^2}\frac{T^{12}_{\lambda=0}}{\sqrt{MM'}}, \quad T_2 = \sqrt{2}\frac{M'}{|\vec{q}|}\left(i\frac{T^{01}_{\lambda=-1}}{\sqrt{MM'}} - \frac{E'}{|\vec{q}|}\frac{T^{23}_{\lambda=-1}}{\sqrt{MM'}}\right), \quad T_3 = \sqrt{2}\frac{M'^2}{|\vec{q}|^2}\frac{T^{23}_{\lambda=-1}}{\sqrt{MM'}}, \tag{C3}$$

with $T_{1,2,3}$ defined in Eq. (B7) and V^{μ}_{λ}, A^{μ}_{λ}, P_{λ} and $T^{\mu\nu}_{\lambda}$ the NRQM matrix elements of the vector, axial, pseudoscalar and tensor $b \to c$ transition currents, respectively. Here, λ is the polarization of the final J/ψ meson. We use states that have well-defined spin in the Z direction in the J/ψ rest frame. Since the J/ψ three-momentum equals $-\vec{q}$ (which is directed along the negative Z axis), λ coincides with minus the helicity, the latter being the same in the c.m. and LAB frames. We obtain the following expressions for the matrix elements:

$$
\begin{aligned}
V^{1}_{\lambda=-1} &= \frac{-1}{\sqrt{2}}\sqrt{2M2E'}\int d^3p\frac{1}{4\pi}[\hat{\phi}^{(J/\psi)}(|\vec{p}|)]^*\hat{\phi}^{(\bar{B}_c)}\left(|\vec{p}-\frac{1}{2}\vec{q}|\right)\sqrt{\frac{\hat{E}_c\hat{E}_b}{4E_cE_b}}\left(-\frac{\frac{1}{2}|\vec{q}|-p_z}{\hat{E}_b}+\frac{-\frac{1}{2}|\vec{q}|-p_z}{\hat{E}_c}\right),\\
A^{0}_{\lambda=0} &= \sqrt{2M2E'}\int d^3p\frac{1}{4\pi}[\hat{\phi}^{(J/\psi)}(|\vec{p}|)]^*\hat{\phi}^{(\bar{B}_c)}\left(|\vec{p}-\frac{1}{2}\vec{q}|\right)\sqrt{\frac{\hat{E}_c\hat{E}_b}{4E_cE_b}}\left(\frac{\frac{1}{2}|\vec{q}|-p_z}{\hat{E}_b}+\frac{-\frac{1}{2}|\vec{q}|-p_z}{\hat{E}_c}\right)\\
A^{1}_{\lambda=-1} &= \frac{1}{\sqrt{2}}\sqrt{2M2E'}\int d^3p\frac{1}{4\pi}[\hat{\phi}^{(J/\psi)}(|\vec{p}|)]^*\hat{\phi}^{(\bar{B}_c)}\left(|\vec{p}-\frac{1}{2}\vec{q}|\right)\sqrt{\frac{\hat{E}_c\hat{E}_b}{4E_cE_b}}\left(1+\frac{2p_x^2-(-\frac{1}{2}\vec{q}-\vec{p})\cdot(\frac{1}{2}\vec{q}-\vec{p})}{\hat{E}_c\hat{E}_b}\right)\\
A^{3}_{\lambda=0} &= \sqrt{2M2E'}\int d^3p\frac{1}{4\pi}[\hat{\phi}^{(J/\psi)}(|\vec{p}|)]^*\hat{\phi}^{(\bar{B}_c)}\left(|\vec{p}-\frac{1}{2}\vec{q}|\right)\sqrt{\frac{\hat{E}_c\hat{E}_b}{4E_cE_b}}\left(1+\frac{2(-\frac{1}{2}|\vec{q}|-p_z)(\frac{1}{2}|\vec{q}|-p_z)}{\hat{E}_c\hat{E}_b}-\frac{(-\frac{1}{2}\vec{q}-\vec{p})\cdot(\frac{1}{2}\vec{q}-\vec{p})}{\hat{E}_c\hat{E}_b}\right),\\
P_{\lambda=0} &= \sqrt{2M2E'}\int d^3p\frac{1}{4\pi}[\hat{\phi}^{(J/\psi)}(|\vec{p}|)]^*\hat{\phi}^{(\bar{B}_c)}\left(|\vec{p}-\frac{1}{2}\vec{q}|\right)\sqrt{\frac{\hat{E}_c\hat{E}_b}{4E_cE_b}}\left(\frac{\frac{1}{2}|\vec{q}|-p_z}{\hat{E}_b}-\frac{-\frac{1}{2}|\vec{q}|-p_z}{\hat{E}_c}\right)\\
T^{12}_{\lambda=0} &= \sqrt{2M2E'}\int d^3p\frac{1}{4\pi}[\hat{\phi}^{(J/\psi)}(|\vec{p}|)]^*\hat{\phi}^{(\bar{B}_c)}\left(|\vec{p}-\frac{1}{2}\vec{q}|\right)\sqrt{\frac{\hat{E}_c\hat{E}_b}{4E_cE_b}}\left(1-\frac{2(-\frac{1}{2}|\vec{q}|-p_z)(\frac{1}{2}|\vec{q}|-p_z)}{\hat{E}_c\hat{E}_b}+\frac{(-\frac{1}{2}\vec{q}-\vec{p})\cdot(\frac{1}{2}\vec{q}-\vec{p})}{\hat{E}_c\hat{E}_b}\right),\\
T^{23}_{\lambda=-1} &= \frac{1}{\sqrt{2}}\sqrt{2M2E'}\int d^3p\frac{1}{4\pi}[\hat{\phi}^{(J/\psi)}(|\vec{p}|)]^*\hat{\phi}^{(\bar{B}_c)}\left(|\vec{p}-\frac{1}{2}\vec{q}|\right)\sqrt{\frac{\hat{E}_c\hat{E}_b}{4E_cE_b}}\left(1-\frac{2p_x^2-(-\frac{1}{2}\vec{q}-\vec{p})\cdot(\frac{1}{2}\vec{q}-\vec{p})}{\hat{E}_c\hat{E}_b}\right),\\
T^{01}_{\lambda=-1} &= \frac{-i}{\sqrt{2}}\sqrt{2M2E'}\int d^3p\frac{1}{4\pi}[\hat{\phi}^{(J/\psi)}(|\vec{p}|)]^*\hat{\phi}^{(\bar{B}_c)}\left(|\vec{p}-\frac{1}{2}\vec{q}|\right)\sqrt{\frac{\hat{E}_c\hat{E}_b}{4E_cE_b}}\left(-\frac{\frac{1}{2}|\vec{q}|-p_z}{\hat{E}_b}-\frac{-\frac{1}{2}|\vec{q}|-p_z}{\hat{E}_c}\right).
\end{aligned}
\tag{C4}
$$

APPENDIX D: RESULTS FOR THE $\bar{B} \to D\tau\bar{\nu}_\tau$ AND $\bar{B} \to D^*\tau\bar{\nu}_\tau$ DECAYS FOR THE CASE OF A POLARIZED FINAL τ

In this Appendix we collect, in Figs. 21–26, results for $\bar{B} \to D\tau\bar{\nu}_\tau$ and $\bar{B} \to D^*\tau\bar{\nu}_\tau$ decays where the final τ has well-defined helicity in the c.m. or LAB frames. All observables have been evaluated with the NP Wilson coefficients of fits 6 and 7 and form factors from Ref. [31].

We obtain predictions that are qualitatively similar to those discussed in Sec. II for $\bar{B}_c \to \eta_c$ and $\bar{B}_c \to J/\psi$ semileptonic decays. We would like to stress that unlike the unpolarized case, where all the accessible observables could be determined either from the c.m. or LAB distributions, in the polarized case, the LAB and c.m. charged lepton helicity distributions provide complementary information. Actually both differential distributions $d^2\Gamma/(d\omega d\cos\theta_\ell)$ and $d^2\Gamma/(d\omega dE_\ell)$ should be simultaneously used to determine the five new independent functions $\mathcal{A}_H$, $\mathcal{B}_H$, $\mathcal{C}_H$, $\mathcal{D}_H$ and $\mathcal{E}_H$, which appear for the case of a polarized final τ [see Eq. (23) of Ref. [33]].

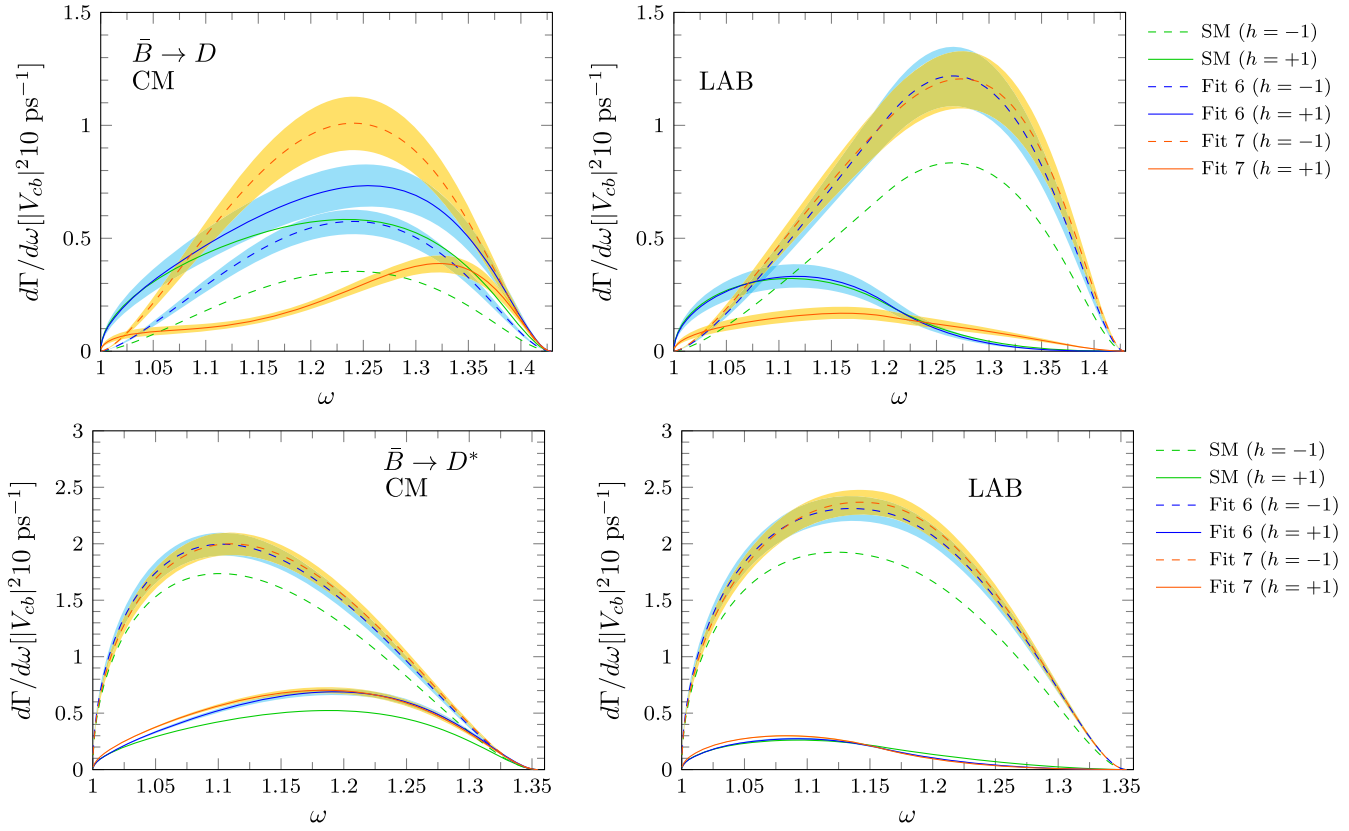

FIG. 21. c.m. (left) and LAB (right) helicity decomposition of the $d\Gamma/d\omega$ differential decay width with a polarized τ. We show distributions for $\bar{B} \to D\tau\bar{\nu}_\tau$ (top) and $\bar{B} \to D^*\tau\bar{\nu}_\tau$ reactions (bottom), which have been evaluated with Wilson coefficients and form factors from Ref. [31]. Uncertainty bands are as in Fig. 16.

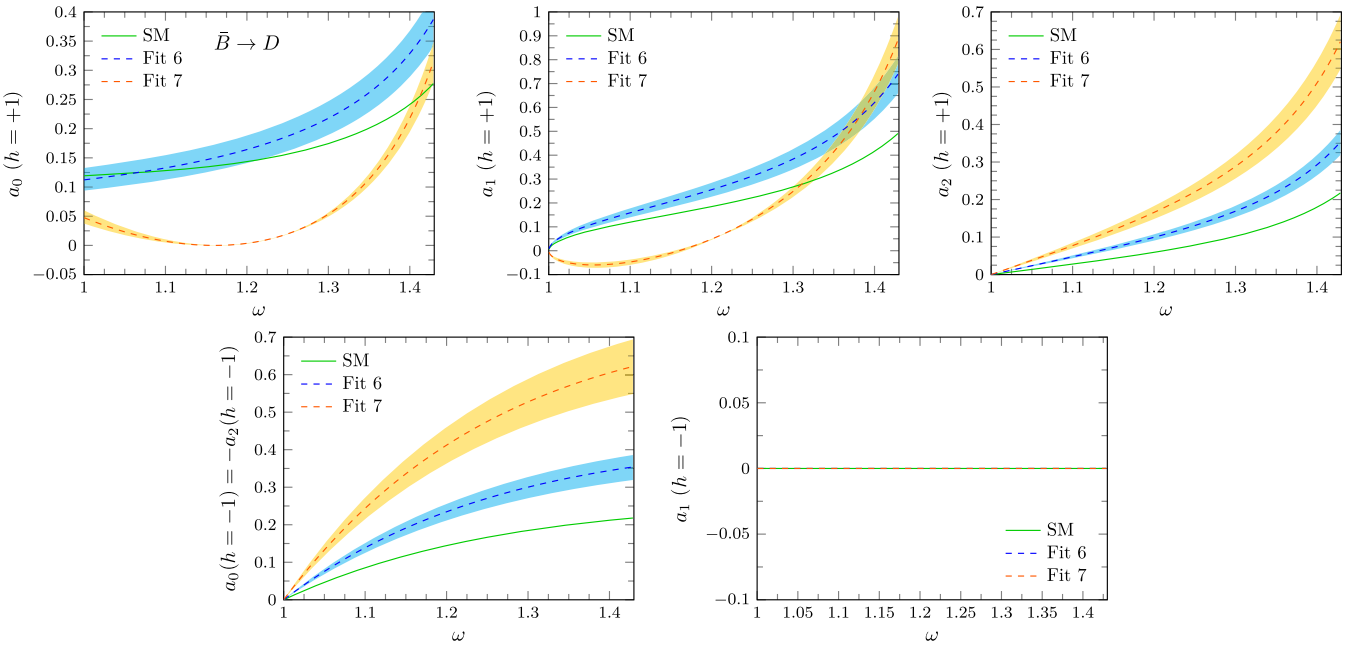

FIG. 22. c.m. angular expansion coefficients for the $\bar{B} \to D\tau\bar{\nu}_\tau$ decay with a polarized τ with positive (upper panels) and negative (lower panels) helicity. They have been evaluated with the Wilson coefficients and form factors from Ref. [31]. Uncertainty bands areas in Fig. 16.

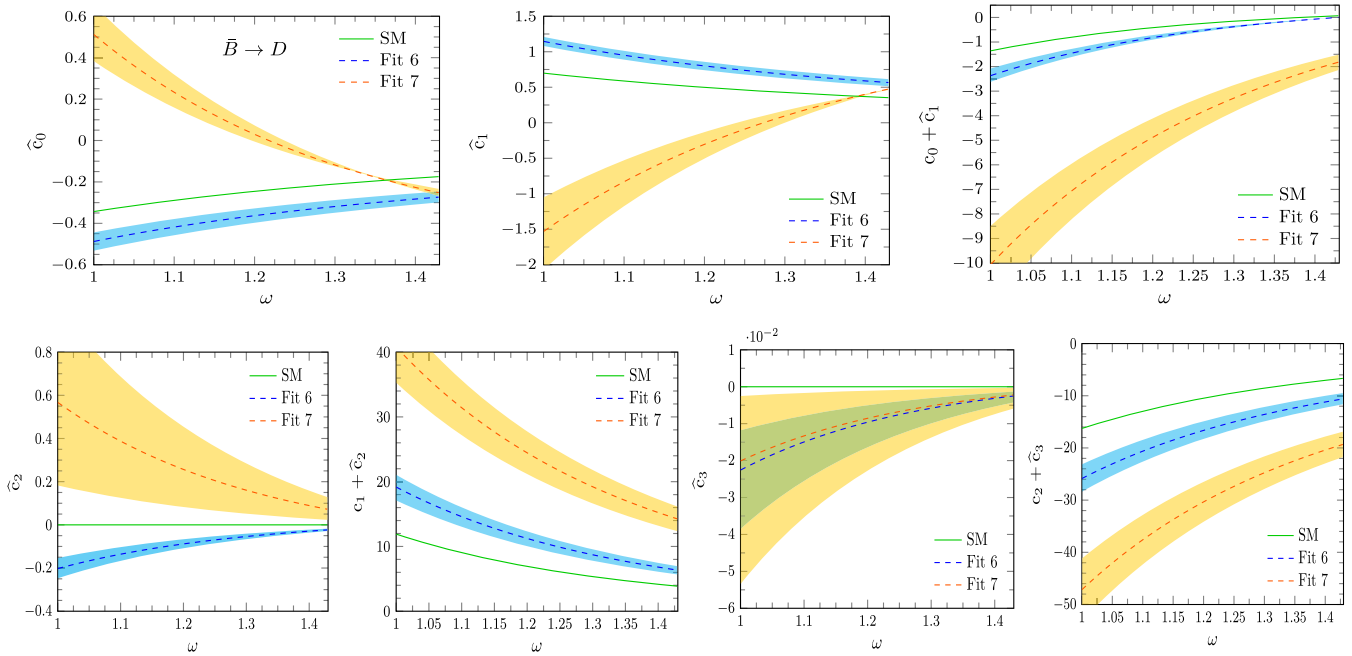

FIG. 23. LAB charged lepton energy expansion coefficients $\hat{c}_{0,1,2,3}(\omega)$ for the polarized $\bar{B} \to D\tau\bar{\nu}_\tau$ decay. We also show the $(c_0 + \hat{c}_1)$, $(c_1 + \hat{c}_2)$ and $(c_2 + \hat{c}_3)$ sums in the third top, second and fourth bottom panels, respectively. All quantities have been evaluated with the Wilson coefficients and form factors from Ref. [31]. Uncertainty bands are as in Fig. 16.

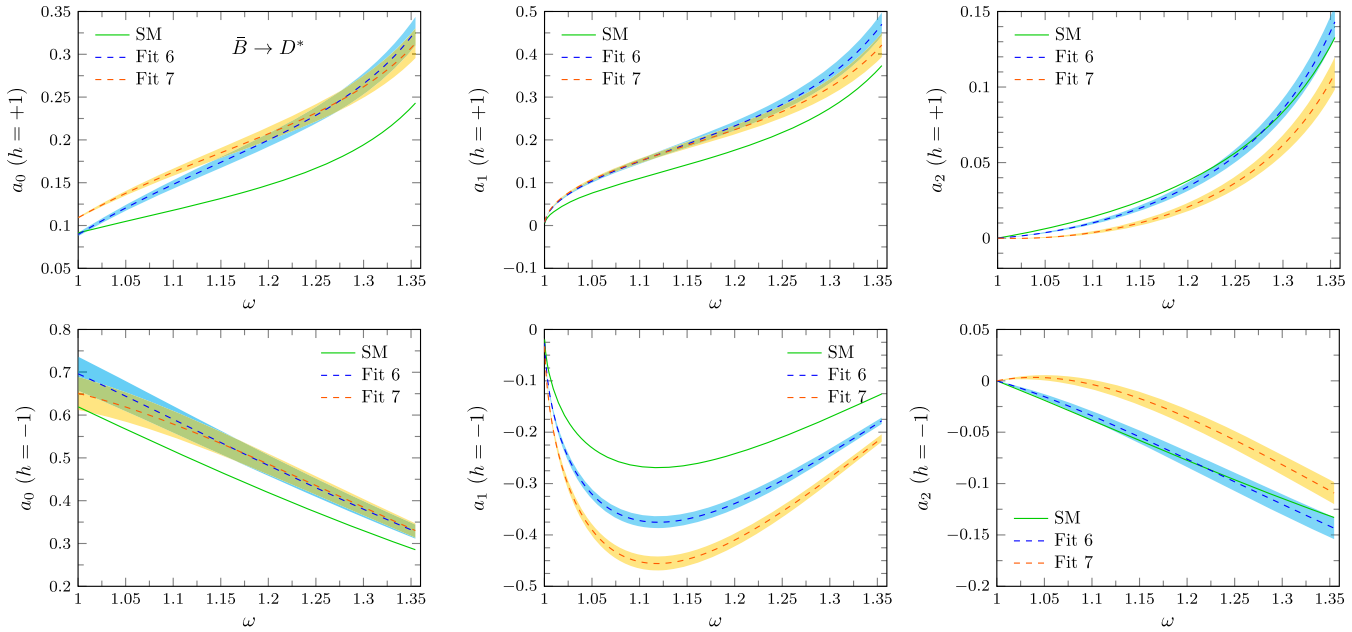

FIG. 24. c.m. angular expansion coefficients for the $\bar{B} \to D^*\tau\bar{\nu}_\tau$ decay with a τ with positive (upper panels) and negative (lower panels) helicity. They have been evaluated with the Wilson coefficients and form factors from Ref. [31]. Uncertainty bands are as in Fig. 16.

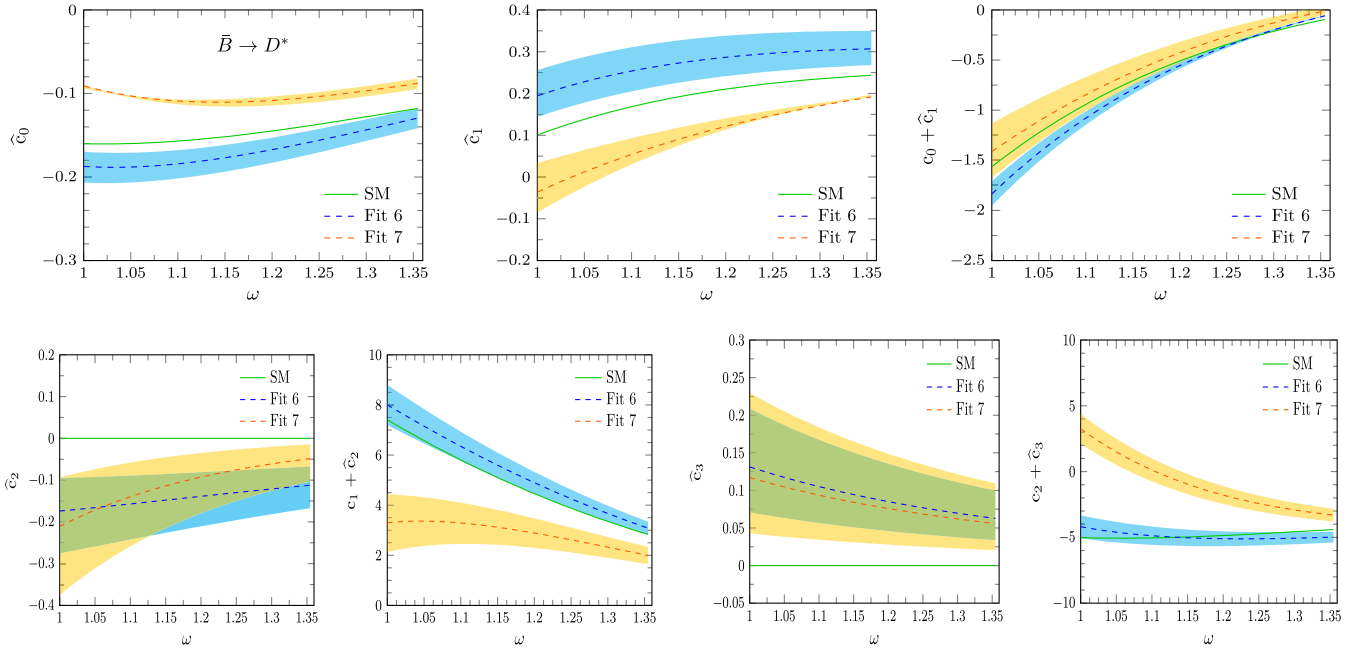

FIG. 25. LAB charged lepton energy expansion coefficients $\hat{c}_{0,1,2,3}(\omega)$ for the polarized $\bar{B} \to D^* \tau \bar{\nu}_\tau$ decay. We also show the $(c_0 + \hat{c}_1)$, $(c_1 + \hat{c}_2)$ and $(c_2 + \hat{c}_3)$ sums in the third top, second and fourth bottom panels, respectively. All quantities have been evaluated with the Wilson coefficients and form factors from Ref. [31]. Uncertainty bands are as in Fig. 16.

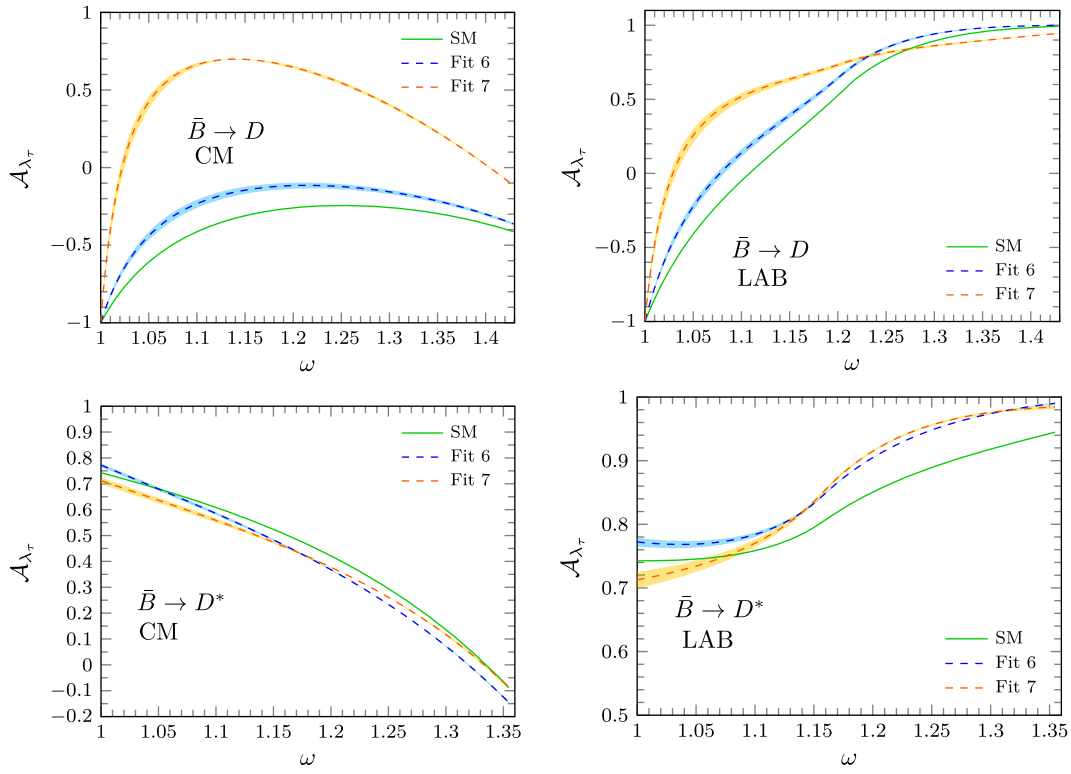

FIG. 26. τ polarization asymmetry $\mathcal{A}_{\lambda_\tau}$ for the $\bar{B} \to D$ (upper panels) and $\bar{B} \to D^*$ (lower panels) semileptonic decays measured in the c.m. (left panels) and LAB (right panels) frames. All quantities have been evaluated with the Wilson coefficients and form factors from Ref. [31]. Uncertainty bands are as in Fig. 16.

[1] Y. S. Amhis *et al.* (HFLAV Collaboration), arXiv:1909.12524.

[2] Y. Amhis *et al.* (HFLAV Collaboration), Eur. Phys. J. C **77**, 895 (2017), online update at https://hflav.web.cern.ch/.

[3] J. P. Lees *et al.* (*BABAR* Collaboration), Phys. Rev. Lett. **109**, 101802 (2012).

[4] J. P. Lees *et al.* (*BABAR* Collaboration), Phys. Rev. D **88**, 072012 (2013).

[5] M. Huschle *et al.* (Belle Collaboration), Phys. Rev. D **92**, 072014 (2015).

[6] Y. Sato *et al.* (Belle Collaboration), Phys. Rev. D **94**, 072007 (2016).

[7] S. Hirose *et al.* (Belle Collaboration), Phys. Rev. Lett. **118**, 211801 (2017).

[8] G. Caria *et al.* (Belle Collaboration), Phys. Rev. Lett. **124**, 161803 (2020).

[9] R. Aaij *et al.* (LHCb Collaboration), Phys. Rev. Lett. **115**, 111803 (2015); **115**, 159901(E) (2015).

[10] R. Aaij *et al.* (LHCb Collaboration), Phys. Rev. Lett. **120**, 171802 (2018).

[11] S. Aoki *et al.*, Eur. Phys. J. C **77**, 112 (2017).

[12] D. Bigi and P. Gambino, Phys. Rev. D **94**, 094008 (2016).

[13] D. Bigi, P. Gambino, and S. Schacht, J. High Energy Phys. 11 (2017) 061.

[14] S. Jaiswal, S. Nandi, and S. K. Patra, J. High Energy Phys. 12 (2017) 060.

[15] F. U. Bernlochner, Z. Ligeti, M. Papucci, and D. J. Robinson, Phys. Rev. D **95**, 115008 (2017); **97**, 059902(E) (2018).

[16] R. Aaij *et al.* (LHCb Collaboration), Phys. Rev. Lett. **120**, 121801 (2018).

[17] A. Yu. Anisimov, I. M. Narodetsky, C. Semay, and B. Silvestre-Brac, Phys. Lett. B **452**, 129 (1999).

[18] M. A. Ivanov, J. G. Korner, and P. Santorelli, Phys. Rev. D **73**, 054024 (2006).

[19] E. Hernández, J. Nieves, and J. Verde-Velasco, Phys. Rev. D **74**, 074008 (2006).

[20] T. Huang and F. Zuo, Eur. Phys. J. C **51**, 833 (2007).

[21] W. Wang, Y.-L. Shen, and C.-D. Lu, Phys. Rev. D **79**, 054012 (2009).

[22] W.-F. Wang, Y.-Y. Fan, and Z.-J. Xiao, Chin. Phys. C **37**, 093102 (2013).

[23] R. Watanabe, Phys. Lett. B **776**, 5 (2018).

[24] A. Issadykov and M. A. Ivanov, Phys. Lett. B **783**, 178 (2018).

[25] C.-T. Tran, M. A. Ivanov, J. G. Körner, and P. Santorelli, Phys. Rev. D **97**, 054014 (2018).

[26] X.-Q. Hu, S.-P. Jin, and Z.-J. Xiao, Chin. Phys. C **44**, 023104 (2020).

[27] D. Leljak, B. Melic, and M. Patra, J. High Energy Phys. 05 (2019) 094.

[28] K. Azizi, Y. Sarac, and H. Sundu, Phys. Rev. D **99**, 113004 (2019).

[29] W. Wang and R. Zhu, Int. J. Mod. Phys. A **34**, 1950195 (2019).

[30] S. Fajfer, J. F. Kamenik, and I. Nisandzic, Phys. Rev. D **85**, 094025 (2012).

[31] C. Murgui, A. Peñuelas, M. Jung, and A. Pich, J. High Energy Phys. 09 (2019) 103.

[32] N. Penalva, E. Hernández, and J. Nieves, Phys. Rev. D **100**, 113007 (2019).

[33] N. Penalva, E. Hernández, and J. Nieves, Phys. Rev. D **101**, 113004 (2020).

[34] R. Aaij *et al.* (LHCb Collaboration), Phys. Rev. D **96**, 112005 (2017).

[35] A. Cerri *et al.*, Report from working group 4: Opportunities in flavor physics at the HL-LHC and HE-LHC, in *Report on the Physics at the HL-LHC, and perspectives for the HE-LHC*, Vol. 7, edited by A. Dainese, M. Mangano, A. B. Meyer, A. Nisati, G. Salam, and M. A. Vesterinen (2019), pp. 867–1158, https://doi.org/10.23731/CYRM-2019-007.867.

[36] J. A. Bailey *et al.* (Fermilab Lattice, MILC Collaborations), Phys. Rev. D **89**, 114504 (2014).

[37] J. A. Bailey *et al.* (Fermilab Lattice and MILC Collaborations), Phys. Rev. D **92**, 034506 (2015).

[38] H. Na, C. M. Bouchard, G. P. Lepage, C. Monahan, and J. Shigemitsu (HPQCD Collaboration), Phys. Rev. D **92**, 054510 (2015); **93**, 119906(E) (2016).

[39] J. Harrison, C. Davies, and M. Wingate (HPQCD Collaboration), Phys. Rev. D **97**, 054502 (2018).

[40] S. Faller, A. Khodjamirian, C. Klein, and T. Mannel, Eur. Phys. J. C **60**, 603 (2009).

[41] M. Neubert, Z. Ligeti, and Y. Nir, Phys. Lett. B **301**, 101 (1993).

[42] M. Neubert, Z. Ligeti, and Y. Nir, Phys. Rev. D **47**, 5060 (1993).

[43] Z. Ligeti, Y. Nir, and M. Neubert, Phys. Rev. D **49**, 1302 (1994).

[44] A. Datta, M. Duraisamy, and D. Ghosh, Phys. Rev. D **86**, 034027 (2012).

[45] M. Duraisamy and A. Datta, J. High Energy Phys. 09 (2013) 059.

[46] M. Duraisamy, P. Sharma, and A. Datta, Phys. Rev. D **90**, 074013 (2014).

[47] Z. Ligeti, M. Papucci, and D. J. Robinson, J. High Energy Phys. 01 (2017) 083.

[48] D. Becirevic, S. Fajfer, I. Nisandzic, and A. Tayduganov, Nucl. Phys. **B946**, 114707 (2019).

[49] S. Bhattacharya, S. Nandi, and S. K. Patra, Eur. Phys. J. C **79**, 268 (2019).

[50] M. Blanke, A. Crivellin, S. de Boer, T. Kitahara, M. Moscati, U. Nierste, and I. Nišandžić, Phys. Rev. D **99**, 075006 (2019).

[51] M. Blanke, A. Crivellin, T. Kitahara, M. Moscati, U. Nierste, and I. Nišandžić, Phys. Rev. D **100**, 035035 (2019).

[52] A. K. Alok, D. Kumar, S. Kumbhakar, and S. U. Sankar, Nucl. Phys. **B953**, 114957 (2020).

[53] S. Jaiswal, S. Nandi, and S. K. Patra, J. High Energy Phys. 06 (2020) 165.

[54] S. Iguro and R. Watanabe, J. High Energy Phys. 08 (2020) 006.

[55] S. Kumbhakar, arXiv:2007.08132.

[56] B. Bhattacharya, A. Datta, S. Kamali, and D. London, J. High Energy Phys. 07 (2020) 194.

[57] R. Dutta and A. Bhol, Phys. Rev. D **96**, 076001 (2017).

[58] V. Kiselev, A. Likhoded, and A. Onishchenko, Nucl. Phys. **B569**, 473 (2000).

[59] V. Kiselev, arXiv:hep-ph/0211021.

[60] T. D. Cohen, H. Lamm, and R. F. Lebed, Phys. Rev. D **100**, 094503 (2019).

[61] B. Colquhoun, C. Davies, J. Koponen, A. Lytle, and C. McNeile (HPQCD Collaboration), Proc. Sci., LATTICE2016 (**2016**) 281 [arXiv:1611.01987].
[62] J. Harrison, C. T. Davies, and A. Lytle (LATTICE-HPQCD Collaboration), arXiv:2007.06957.
[63] J. Harrison, C. T. Davies, and A. Lytle (LATTICE-HPQCD Collaboration), arXiv:2007.06956.
[64] C. Semay and B. Silvestre-Brac, Z. Phys. C **61**, 271 (1994).
[65] B. Silvestre-Brac, Few-Body Syst. **20**, 1 (1996).
[66] R. Bhaduri, L. Cohler, and Y. Nogami, Nuovo Cimento A **65**, 376 (1981).
[67] Y. Sakaki, M. Tanaka, A. Tayduganov, and R. Watanabe, Phys. Rev. D **91**, 114028 (2015).
[68] P. Asadi, M. R. Buckley, and D. Shih, J. High Energy Phys. 09 (2018) 010.
[69] A. Greljo, D. J. Robinson, B. Shakya, and J. Zupan, J. High Energy Phys. 09 (2018) 169.
[70] D. J. Robinson, B. Shakya, and J. Zupan, J. High Energy Phys. 02 (2019) 119.
[71] A. Azatov, D. Barducci, D. Ghosh, D. Marzocca, and L. Ubaldi, J. High Energy Phys. 10 (2018) 092.
[72] J. Heeck and D. Teresi, J. High Energy Phys. 12 (2018) 103.
[73] P. Asadi, M. R. Buckley, and D. Shih, Phys. Rev. D **99**, 035015 (2019).
[74] K. Babu, B. Dutta, and R. N. Mohapatra, J. High Energy Phys. 01 (2019) 168.
[75] D. Bardhan and D. Ghosh, Phys. Rev. D **100**, 011701 (2019).
[76] R.-X. Shi, L.-S. Geng, B. Grinstein, S. Jäger, and J. M. Camalich, J. High Energy Phys. 12 (2019) 065.
[77] J. D. Gómez, N. Quintero, and E. Rojas, Phys. Rev. D **100**, 093003 (2019).
[78] R. Mandal, C. Murgui, A. Peñuelas, and A. Pich, J. High Energy Phys. 08 (2020) 022.
[79] B. Aubert *et al.* (*BABAR* Collaboration), Phys. Rev. D **79**, 012002 (2009).
[80] M. Neubert, Phys. Rep. **245**, 259 (1994).
[81] E. E. Jenkins, M. E. Luke, A. V. Manohar, and M. J. Savage, Nucl. Phys. **B390**, 463 (1993).